ELSEVIER

Journal of Structural Geology 30 (2008) 116–136

JOURNAL OF STRUCTURAL GEOLOGY

www.elsevier.com/locate/jsg

Slip partitioning and inclined dextral transpression along the Zagros Thrust System, Iran

Khalil Sarkarinejad*, Ahmad Azizi

Department of Earth Sciences, College of Sciences, Shiraz University, Shiraz 71454, Iran

Received 1 January 2007; received in revised form 4 October 2007; accepted 18 October 2007
Available online 5 November 2007

Abstract

Flexural duplex structures and shear zones are well developed in the Heneshk area, in southwestern Iran. The Zagros Thrust System in this area consists of eight sheets of NW-striking, NE-dipping dextral strike-slip duplexes that are linked with imbricate fans and oblique-slip thrusts. The Zagros Thrust System is a portion of the internal zone of the Zagros orogenic belt. This internal zone is characterized by penetrative plastic deformation and metamorphism. Based on the kinematic vorticity number ($W_k = 0.73 \pm 0.02$) calculated from quartz porphyroclasts of the Goshti shear zones along the Zagros Thrust System, the estimated θ angle between the maximum instantaneous strain axis (ISA) and the transpressional zone boundary is 33°. The estimated α angle of the plate convergence or the flow apophysis of the displacement field is 25°.The presence of dominantly dextral shear sense indicators in the area is consistent with dextral inclined transpressional convergence. The mean estimated finite deformation (W_m) value indicates relative contributions of 47% pure shear and 53% simple shear for the deformation which involved both strike-slip and oblique slip displacements. In this inclined transpression, about 40% strike-slip partitioning was required to accommodate the finite strain and re-orientation of instantaneous strain.

Keywords: Zagros Thrust System; Transpression; Shear zone; Zagros orogenic belt; Iran

1. Introduction

Zones of oblique convergence have been the subject of extensive geodynamical and strain modeling (Fig. 1). Sanderson and Marchini (1984) proposed a three-dimensional model (Fig. 1a) where a vertical shear zone undergoes strike-slip and the zone thins (transpression) or thickens (transtension) in response to zone-normal compression or extension. Their model predicts that, for a vertical transpressional shear zone, the maximum principal finite strain axis will be either horizontal or vertical. Fossen and Tikoff (1993) and Tikoff and Fossen (1993) expanded the model of Sanderson and Marchini (1984) by expressing flow kinematic quantities, such as the kinematic vorticity number and finite strain axes, in terms of finite strain parameters for steady-state deformation conditions. Jones et al. (2004) developed a mathematical description of inclined transpression (Fig. 1b and c) by extending the model of Sanderson and Marchini (1984) to consider non-vertical deformation zones, but they retained the assumptions of the idealized boundary conditions. In their model, deformation is homogeneous, constant volume, laterally and basically confined, and occurs between parallel zone boundaries. In both Fig. 1b and c, the vector of finite zone boundary displacement lies oblique to all three principal planes of the Cartesian coordinate system (Jones et al., 2004).

The kinematic vorticity number (W_k) is defined as the nonlinear ratio of pure shear and simple shear components of deformation, ranging from zero for coaxial (pure) shear to one for non-coaxial (simple) shear, assuming steady-state deformation (Means, 1994; Law et al., 2004). Pure shear and simple shear make equal contributions to the instantaneous flow at $W_k = 0.71$ (Law et al., 2004). In transpressional zones, the simple shear component accommodates discrete slip on strike slip faults. For plate motion which is dominated by normal to

* Corresponding author. Tel.: +98 711 832 1348; fax: +98 711 228 4572.
E-mail address: sarkarinejad@geology.susc.ac.ir (K. Sarkarinejad).

0191-8141/$ - see front matter © 2007 Elsevier Ltd. All rights reserved.
doi:10.1016/j.jsg.2007.10.001

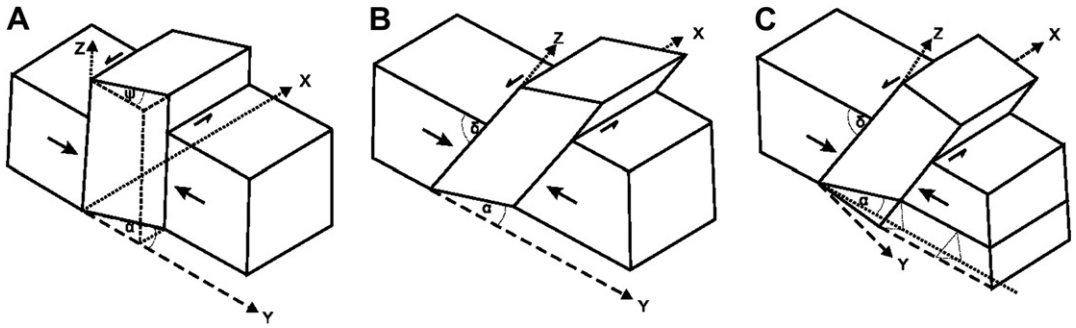

Fig. 1. (A) 3D Vertical transpression zone, from Sanderson and Marchini (1984), in which material within the boundaries is allowed to slip freely in the vertical direction with constant volume. (B) Inclined transpression zone, from Jones et al. (2004), in which displacement of the undeformed zone bounding blocks with respect to one another occurs entirely in the horizontal plane. (C) Oblique transpression zone (Fossen and Tikoff, 1993; Tikoff and Teyssier, 1994) in which the original model of transpression has been changed to analyze the effects of simultaneous pure and simple shearing.

moderately oblique convergence (Fig. 1c), W_k of the transpressional zone decreases almost linearly with increasing partitioning of the strike-slip component (Tikoff and Teyssier, 1994).

Robin and Cruden (1994) developed a continuum mechanics model in which the ''transpressed'' rock is a linear viscous material squeezed upward between two parallel, rigid, vertical walls. Fabrics observed in natural shear zones agree with the theoretical arguments from continuum mechanics (Jiang et al., 2001). Jones et al. (2004) argue that natural deformation of rocks rarely conforms to the idealized assumptions used in mathematical models. The boundary conditions of models are simplistic in comparison with the deformation in real shear zones.

Despite the importance of developments in the numerical simulation of transpression (i.e. Tikoff and Fossen, 1993, 1999; Dutton, 1997; Jiang and Williams, 1998; Passchier, 1998) or inclined transpression (Jones et al., 2004) and progressive development of strain and deformation fabrics in such zones (i.e. Tikoff and Fossen, 1993, 1999; Dutton, 1997; Jiang and Williams, 1998; Passchier, 1998; Jones et al., 2004), detailed field structural studies combined with microstructural and quartz *c*-axis fabric data along real transpression zone boundaries such as Zagros Thrust System are needed to improve our understanding of the complex behavior of materials in high strain zone.

The objectives of this paper are: (1) to examine field structural data from the Zagros Thrust System of the Zagros Orogenic Belt; (2) to investigate the quartz *c*-axis preferred orientations within quartz mylonites and quartz ribbon mylonites and other microstructures of the deep-seated Zagros sole thrusts or basal shear zones; (3) to present mean kinematic vorticity numbers, mean finite strain data and *k*-values; and (4) to establish the relationship between the estimated kinematic vorticity number, *k*-value, pure-shear, simple-shear components, and stretching lineation to present a 3D model for this transpressional zone.

2. Regional geological settings

The studied strike-slip duplex structures and shear zones are located in the northeast of the city of Dehbid in the province of Fars in southwestern Iran. These structures are part of the ''Main Zagros Thrust Zone'' and the Sanandaj–Sirjan metamorphic Zone (Fig. 2; Stöcklin, 1968; Berberian and King, 1981; Alavi, 1994). They form part of the Zagros orogenic belt, which is located in the central part of the Alpine-Himalayan Mountain Range and extends for more than 1500 km in a NW–SE direction from eastern Turkey to the Minab–Zendan fault system in southern Iran (Hynes and McQuillan, 1974; Stöcklin, 1974). This belt results from the closure of the Neo-Tethyan Ocean due to northeast-dipping subduction of oceanic crust below the Iranian microcontinent (Berberian and King, 1981; Berberian et al., 1982; Alavi, 1994). The subducted and obducted Neyriz ophiolite in the south of the Neo-Tethyan Ocean was created by three NW–SE trending fast-spreading diapirs and segmented by a dextral palaeo-transform fracture zone (Sarkarinejad, 2003, 2005). The obducted, well-exposed and well-preserved mantle section forming the Neyriz ophiolite (Sarkarinejad, 2005) runs parallel to the ''Main Zagros Thrust Zone'' and forms part of the Zagros Suture Zone. Along this suture, passive Afro-Arabian and active Iranian continental margins of the Neo-Tethyan Ocean collided.

The Ar^{40}–Ar^{39} spectrum obtained from the biotite layer in a garnet amphibolite sequence associated with basic and ultrabasic rocks of the Neyriz ophiolite suggests that the age of initial emplacement of the ophiolite was Middle Jurassic (170 Ma) with further emplacement and metamorphism in the Late Cretaceous (97 Ma; Hynes and Reynolds, 1980).

K^{40}–Ar^{40} cooling ages of separate amphiboles, muscovite from amphibolites and muscovite schist associated with the Sanandaj–Sirjan metamorphic belt in the Neyriz area, southwestern Iran, suggest dates of 175.8 ± 5.1–124.0 ± 6.9 Ma and 105.8 ± 6.0–93.5 ± 2.2 Ma (Sheikholeslami et al., 2003).

Based on analysis of global sea-floor spreading, fault systems and earthquake slip vectors (NUVEL-1A plate tectonic model), the Arabian plate is moving N13°E at a rate of about 31 mm yr^{-1} relative to Eurasia at the longitude of 52° E (DeMets et al., 1990, 1994). McQuarrie et al. (2003) suggest a fairly constant rate of 20–30 mm yr^{-1} of convergence since 59 Ma. Vernant et al. (2004), based upon GPS sites fixed in the central Iranian block, suggest that the main direction of shortening is roughly north–south with decreasing convergence

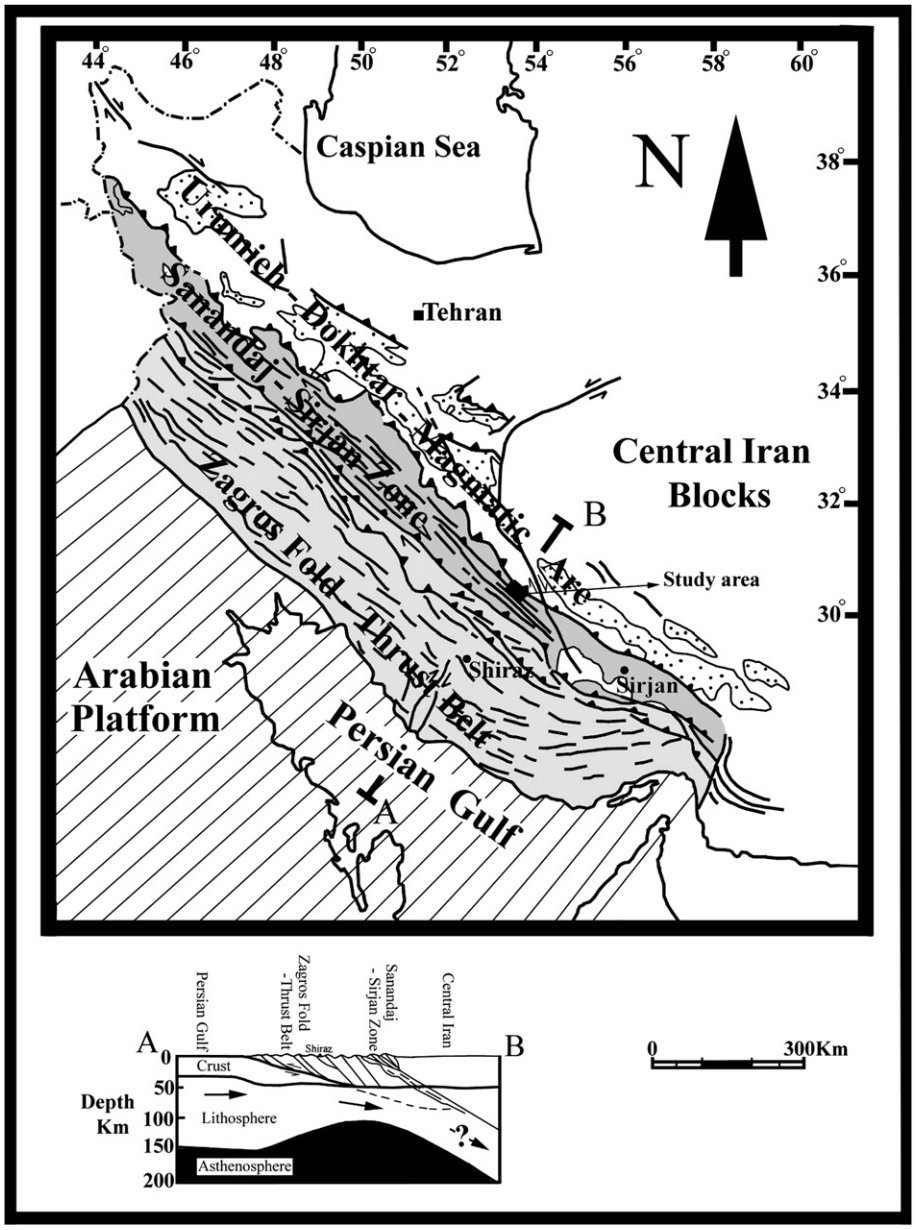

Fig. 2. Tectonic map of the Zagros orogenic belt with sub-divisions according to Stöcklin (1968), Berberian and King (1981) and Alavi (1994). The Zagros orogenic belt includes the Urumieh-Dokhtar Magmatic Arc, the Sanandaj–Sirjan metamorphic belt and the Zagros Fold-and-thrust belt.

rate from 9 ± 2 mm yr^{-1} in the southeastern Zagros to 4.5 ± 2 mm yr^{-1} in the northwestern part of the range.

Isoseismal regions of moderate to large magnitude earthquakes in the Zagros are localized along the deep-seated master thrust faults bordering the morphotectonic units of the Zagros. These thrusts are classified as the ''Main Zagros Reverse Fault'' (MZRF) and the ''Main Recent Fault'' (MRF), recent faults and thrusts exposed at the surface (Berberian, 1995). The Main Zagros Reverse Fault is a major seismically active right-lateral strike-slip fault striking NW–SE (Tchalenko and Braud, 1974; Berberian, 1995; Berberian and Yeats, 2001).

The Sanandaj–Sirjan paired metamorphic belts contain (i) HP-LT metamorphic rocks (Alpine-type) that consist of amphibolite, eclogite, blueschist, kyanite schist and (ii) a parallel zone of HT-LP metamorphic rocks (Abukuma-type) which consist of medium to high-temperature metamorphic rocks including sillimanite schist, cordierite schist and hornfels (Sarkarinejad, 1999). This part of the Zagros belt is dominated by either large-scale composite duplex structures or low- to high-angle NE-dipping imbricate systems (Alavi, 1994).

The metamorphic belt was uplifted during the late Cretaceous continental collision between the Afro-Arabian continent and the Iranian microcontinent (Alavi, 1994; Mohajjel and Fergusson, 2000). The metamorphic rocks of the area consist of thin-bedded crystalline dolomitic limestone, slate, phyllite, phyllonite and mylonite near the villages of Goushti and Heneshk (Fig. 3) and the Kowlikosh metamorphic complex. The Kowlikosh metamorphic complex consists of mica schist, calc schist, marble, metasandstone, metavolcanic rocks and metamorphosed basic and acidic intrusive rocks (Shahidi et al., 1999).

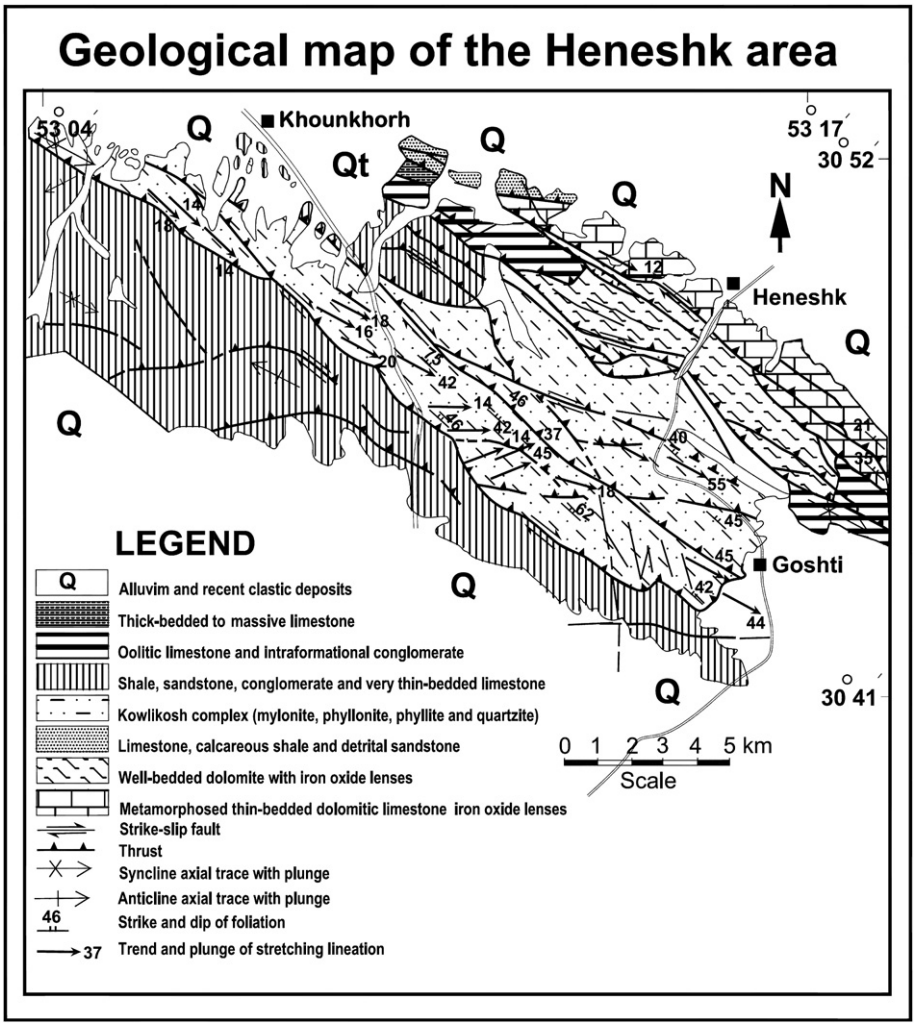

Fig. 3. Modified geological map of the Heneshk area showing the distribution of the Kowlikosh complex which consists of phyllite, phyllonite, mylonite, quartz mylonite and metamorphosed dolomitic limestone.

3. Outcrop scale structures

3.1. Slaty cleavage and schistosity

Most of the S-tectonites of the Heneshk phyllite belt of the mapping area consist of phyllite, mica schist, quartz veins, thin-bedded crystalline limestone, calc schist, phyllonite, quartz–feldspar mylonite and quartz-derived mylonite (Fig. 3). The phyllite belt is 23 km long and 2–6.5 km wide and extends along the ''Main Zagros Thrust Zone'' in a NW–SE direction. Most phyllite in the belt displays overprinting foliations. The ''main foliation'' of the phyllite and mica-schist is recognized as a continuous schistosity which is characterized by planar fabric elements of layer silicates or flattened/stretched grains that have a preferred orientation and are distributed throughout the rocks (Marshak and Mitra, 1988). Measurements of the ''main foliation'' show a mean strike of N27° W, 21° NE. This foliation (S1) is sub-parallel to parallel with the ''Main Zagros Thrust Zone''. The strong main foliation (S1) was formed during the first deformation phase (D1). This foliation is overprinted by the second foliation (S2) which is defined by compositional layering and preferred orientation of platy minerals (e.g. muscovite). The S2 foliation usually forms crenulation cleavages, which consist of symmetrical and asymmetrical microfolds. The orientation of S2 varies from S30° W to S53° W. S1 and S2 are oriented at an angle of 60° to 70° on the microscopic scale. Typically, S2 has a relatively constant NE-SW orientation, which changes only modestly from one location to another. The third phase of deformation (D3) is developed along the shear zones and thrusts and gives rise to the formation of S/C shear band cleavages (S3). Mica preferred orientation or compositional layering may be transected at small angles by a set of sub-parallel micro-shear zones. Such minor shear zones are known as shear bands and the complete structure forms a shear band cleavage (Berthe et al., 1979b; White, 1979; Gapais and White, 1882).

3.2. Asymmetrical folds

Small-scale and large-scale asymmetrical folds (Fig. 4a) to the east of the Heneshk area are associated with the thrust

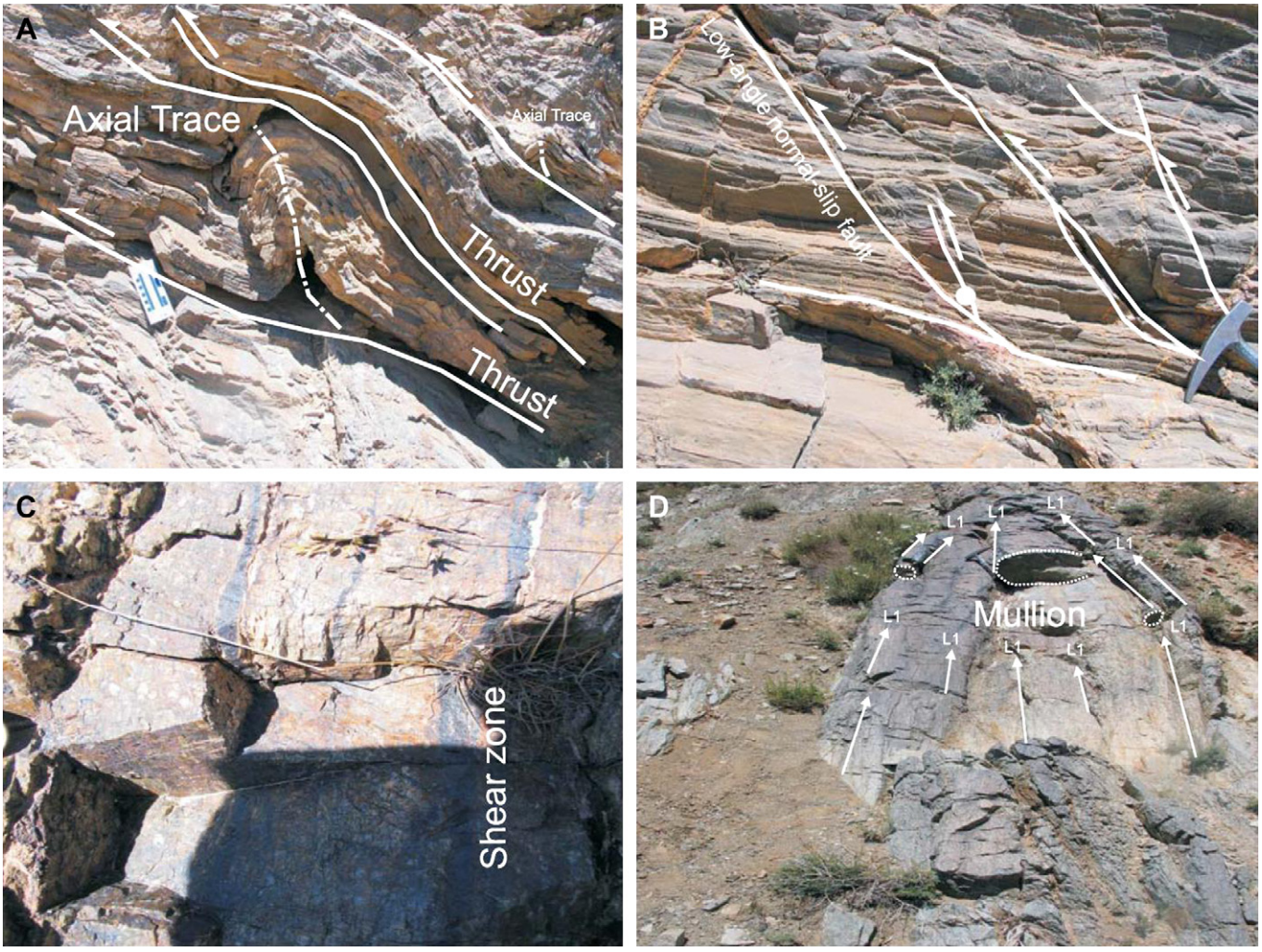

Fig. 4. (A) Small-scale asymmetrical fold in the east of the Henashk area is associated with the Zagros Thrust System. The asymmetrical fold is classified as sub-asymmetrical ($0 < DA < 3$). (B) Low-angle normal-slip faults which are initiated near the stratigraphic base and rotated progressively upwards to form curved fault planes in the metamorphosed thin-bedded dolomitic limestone near the Heneshk village. (C) A1 shear zone showing porphyroclast systems. (D) Mullions showing L1 stretching lineation.

system that typically has a ramp-flat geometry. Suppe (1985) has emphasized that movement along a flat (i.e., a flat-fault segment parallel to bedding) is not reflected in stratigraphic separation until the hanging-wall flat moves onto another unit at the footwall ramp. Several kinematic models have been advanced to explain asymmetrical fold origins: the fold-bend fault model relates fold development to movement over thrust ramps (Suppe, 1983), and the fault-propagation fold model links fold amplification to growth and propagation of blind thrusts (Suppe, 1985).

The asymmetric folds are in predominantly Permian thin-bedded metamorphosed dolomitic limestone, phyllite and phyllonite. The presence of muscovite in the phyllite and phyllonite indicates that they were metamorphosed up to greenschist facies conditions. Asymmetrical folds in the metamorphosed dolomitic limestone are classified as class 2 or similar folds (Ramsay, 1967) and those in the phyllite and phyllonite are classified as class 2 and 3 folds. The thin-bedded dolomitic limestone was thrust over well-bedded dolomite that contains iron oxides lenses (Shahidi et al., 1999). The folds show different generations. The first generations of the asymmetrical folds (F1) have an axial plane orientation of N37° W, 84° NE, parallel with the thrusts and shear zones. They are asymmetric and generally vary from recumbent to gently or moderately inclined, based on their NW-trending NE-dipping axial planes. The folds show an axial plane trend of N52°W, 87° SW.

Most of the folds are non-cylindrical and asymmetric (Fig. 4a). Their profiles have no mirror plane of symmetry and their limbs are of unequal length (Twiss and Moores, 1992). The degree of asymmetry of the folds in the area was determined according to the methods of Ramsay and Hubber (1987) and Tripathi and Gairola (1999). Tripathi and Gairola (1999) proposed a method quantifying the asymmetry of folded surfaces between two consecutive inflection points and measured the degree of asymmetry using Fourier analysis of fold profiles. The degree of asymmetry (DA) of folded surfaces is a function of two variables. These variable components are a shape component (Δshape) and a size component (Δsize): $DA = \Delta\text{shape} + \Delta\text{size}$.

Based on the above derivation, asymmetrical folds in phyllite and phyllonite are classified as extremely asymmetrical (DA < 12) whilst symmetrical folds have DA = 0 and moderately asymmetrical folds have 6 < DA < 9. Folds in the metamorphosed dolomitic limestone are classified as sub-asymmetrical (Fig. 4a; 0 < DA < 3). In extremely and moderately asymmetrical folds in phyllonite, quartzite layers and boudins in the limbs are enveloped by sheet silicate layers and display a history of progressive deformation and rotation. These quartzite boudins have been lengthened at the initial stage of deformation forming pinch-and-swell structures and drawn boudins (Goscombe et al., 2004). The drawn boudins and pinch-and-swell structures were asymmetrically shortened and sheared by convergence at the final stage. Many boudins are asymmetrical and are potential shear sense indicators (Goscombe and Passchier, 2003). A dextral sense of shear is indicated by all the rotational and movement parameters in the boudins as well as the C-type and S-type shear band cleavages (Lister and Snoke, 1984) and flanking asymmetrical folds (Hudleston, 1999).

3.3. Stretching lineation

Various types of stretching lineations formed in the Heneshk area during ductile deformation, including a stretching lineation in the mylonite defined by the long axes of ellipsoidal quartz grains and long narrow quartz ribbons, mesoscopic fold hinge lines and fold mullions (Fig. 4d). The mean plunge and trend of the stretching lineation of elongated quartz grains is 16°, S64°E to 32°, S66°E and the main trend of the L1 stretching lineation is NW–SE throughout the area.

3.4. Mullions

Formation of mullions near the village of Heneshk is related to folding and thrusting of the thin-bedded metamorphosed and recrystallized limestone in contact with phyllite, phyllonite and quartz–feldspar mylonite (Fig. 4d). Metamorphosed limestone and quartz–feldspar mylonite appear to be more competent than the phyllite. Mullions form regular cylindrical surfaces which are convex toward the incompetent phyllite. The mean orientation of the mullion plunge and trend is 24°, S63°E.

4. Thrust and fold structures

Several fault-bend folds and thrusts crop out near the road cut to the Heneshk village in the north of Dehbid city. The road cuts are oriented approximately perpendicular to the strike of the fault-bend fold structures and thrusts and present cross-sectional views of these structures (Fig. 5). The fault-bend fold structures are imbricate stacks of NW-striking, NE- and SW-dipping parallel sheets of thrusts containing thin and thick-bedded nodules of cherty metamorphosed Permian dolomitic limestone (Shahidi et al., 1999), phyllite, phyllonite and mylonite. The ‘‘Main Zagros Thrust Zone’’ consists of the eight thrust sheets with development of the several imbricate thrusts connecting straight thrust segments. The Heneshk fault-bend folds are part of the internal zone of the hinterland Zagros Orogenic Belt. The internal zone is part of the metamorphic belt in which plastic deformation dominates and penetrative strain developed (Marshak and Mitra, 1988). It is referred to as the hinterland. The Heneshk thrust system contains all the elements that are consistent with hinterland-dipping duplexes. In these duplexes, thrusts faults are highly irregular, resulting either from intersection of shallow NE-dipping faults with irregularities of topography or from folding of the fault surfaces. The duplexes range in scale from centimeter to several hundred meters and mainly consist of thin-bedded metamorphosed dolomitic limestone (3 mm to 7 cm thick), phyllite, phyllonite, mylonite, calc-schist and slightly metamorphosed sandstone. The thin-bedded metamorphosed dolomitic limestone is repeated by imbrications. Like many fractal phenomena with scale invariance, the geometry of the small and large-scale imbrications of the area duplexes is similar. They display the sigmoidal shape of horses with planar or gently curved floor and roof thrusts bounding the duplexes. Some small-scale duplexes in the metamorphosed dolomitic limestone are up to 133 cm long and contain up to 14 horses (Fig. 6). This indicates that the Heneshk thrust systems can be classified as typical flexural-slip duplexes that can be compared with those of well-documented duplexes from other thrust belts such as the Makran accretionary prism of southwest Pakistan (Platt and Leggeth, 1986), and duplexes from the Eriboll area of the Moine Thrust zone, in northwest Scotland (Bowler, 1987) and from the Lewis Thrust sheet in the Canadian Rocky Mountains (McClay and Insley, 1986).

The metamorphosed dolomitic limestone is characterized by the presence of quartz and carbonate fiber veins and pressure fringes. The fibers are parallel with the floor and roof of link thrusts. Pressure fringes of calcite and quartz fibers are mostly face-controlled in which the geometry of the fiber growth depends on the shape of faces of pyrite grains. These fringes are sub-divided into three small segments according to their growth orientation. The L1 orientations, which consist of composite calcite and quartz, display D1 deformation with a NW–SE orientation. This is parallel with the S1 foliation. L1 stretching lineations that consist of up to 70% quartz grains have a NW–SE orientation.

4.1. Normal faults

In the east of the Heneshk area, there are several mesoscale compressional low-angle normal-slip faults that cut and drag the horizontal strata of the thin-bedded metamorphosed dolomitic limestone. They cut thrusts that are associated with the ‘‘Main Zagros Thrust Zone’’. The normal fault planes are rotated progressively to form curved fault planes (Fig. 4b).The fault strike is N30°W and the dip at the base is 10° NE but it progressively changes up to 70° NE. The low-angle normal-slip faults show characteristics of oblique-slip faults. The slip on faults initiates near the base of steeply dipping fault segments and propagates upward towards the ground surface, and downwards and laterally along the low-angle detachment (Ofoegbu and Ferrill, 1998). These types

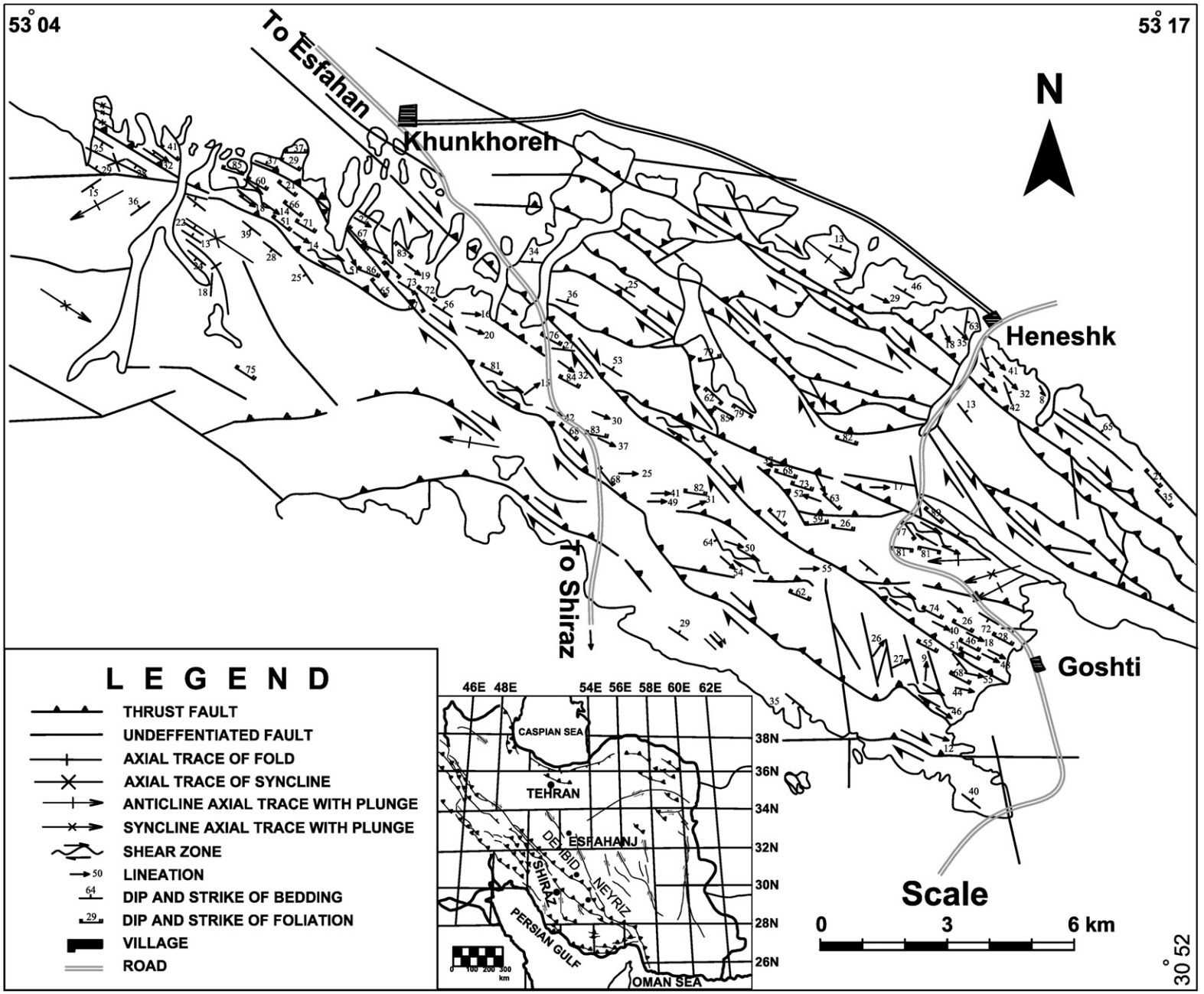

Fig. 5. Structural map showing the Zagros Thrust System in the Heneshk area. The system contains all elements that are consistent with the hinterland-dipping duplexes. Link thrusts, horse stocks, bedding and foliations dip towards the hinterland of the Zagros Thrust System.

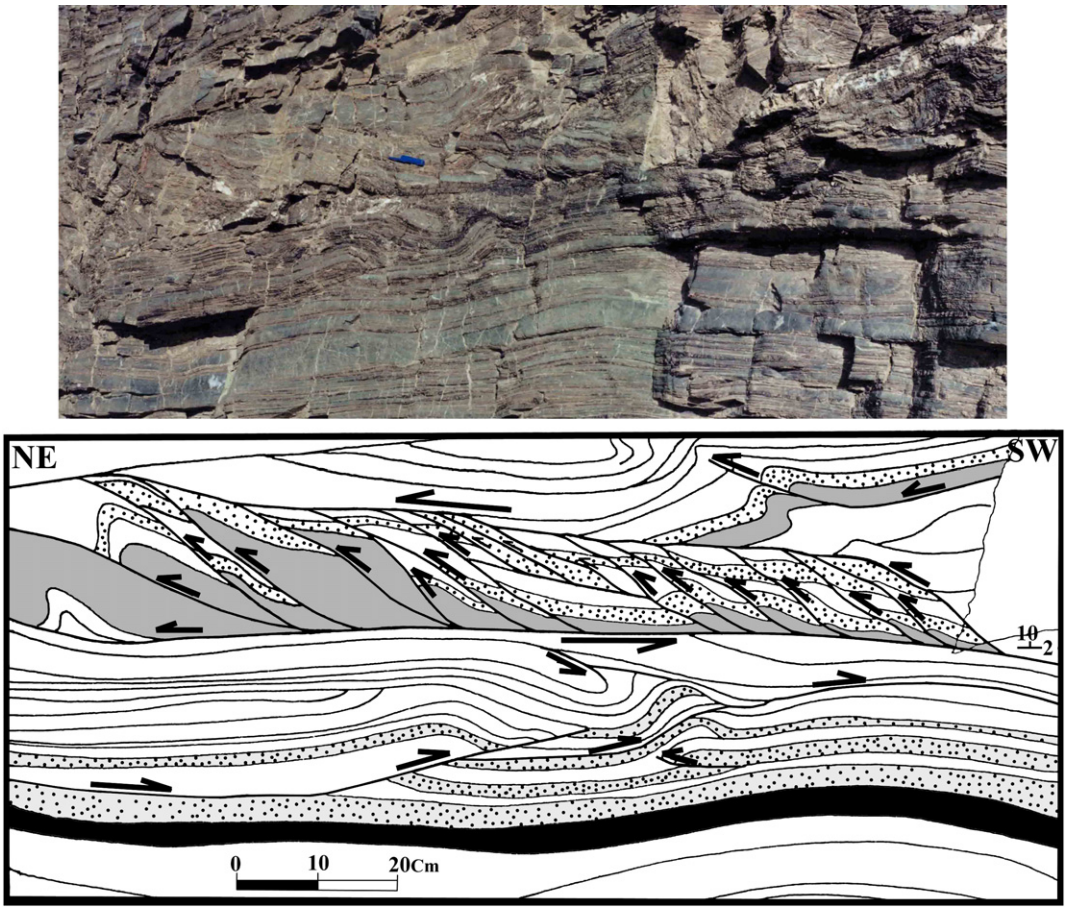

Fig. 6. Photograph and cross section of the flexural-slip duplex structures showing sigmoidal shape of the rotated horse stocks within planar or gently curved floor and roof thrust geometry, which may be interpreted as indicating synchronous thrust movement to the northeast direction.

of normal faults are parts of the deep-seated master thrust faults that are classified as the Master Recent Fault (MRF; Berberian, 1995). The onset of slip along the MRF is interpreted to have been accompanied by a change in the regional stress regime from dominantly thrust slip to right-lateral slip (Authemayou et al., 2006). Low-angle normal faults are credible sources of seismic risk, but it is smaller than the risk associated with steeply dipping faults because of the reduced rupture propagation rate on low-angle faults (Ofoegbu and Ferrill, 1998).

5. Structures of the shear zones

Four shear zones are recognized in the Heneshk area (Fig. 7). They are exposed along the flexural-slip duplexes and cut through the Kowlikosh metamorphic complex. These four shear zones are named A_1, A_2, A_3 and A_4, and they are associated with the strike-slip ''Main Zagros Thrusts Zone'' (Figs. 2, 5 and 7). A_1, A_2 and A_4 are aligned along the thrust near the Goshty village. They possibly form a single shear zone. The A_4 shear zone is in contact with the Middle to Late Jurassic thin bedded, shale, sandstone and thin-bedded limestone. They are segments of the ''Main Zagros Thrust Zone''. The well exposed NW–SE main shear zones of A1 and A2 are located in the southeast of the Goshti village and consist of quartz–feldspar-muscovite mylonite, quartzitic mylonite and calc mylonite. The Goshti shear zone is 6.5 km long and 10 to 470 m wide. Its planar shape fabric or more specifically its mylonitic foliation (Passchier and Trouw, 2005) or shape preferred orientation is oriented N10°W, 21° NE to N45° W, 80° NE. The planar shape fabric is defined by C-plane shear bands in a quartz–feldspar-muscovite mylonite which displays well-developed quartz lattice-preferred orientations (LPO). The quartzite mylonite commonly forms domino, rotated shear band boudins and drawn boudins (Goscombe et al., 2004), within phyllonitic fold limbs. The shear band cleavage in mylonite and phyllonite consists of S-planes transected by C-planes (Berthe et al., 1979a,b; Lister and Snoke, 1984) forming the C/S shear band cleavages which are best observed on the mesoscopic-scale (Fig. 8) parallel to the stretching lineation (*XZ* plane in the shear zone). The A_1 and A_2 foliations display NW–SE trends and are NE-dipping, but the A_3 and A_4 mylonitic foliation trends show greater variability as a result of curvature of the shear zones. The mean foliation orientation of all shear zones is S57°E, 75 NE (Fig. 7). The geometry of the S–C shear band cleavages indicates a dextral sense of shear.

The stretching lineation in the mylonite is defined by the long axes of ellipsoidal quartz grains and long narrow stripes

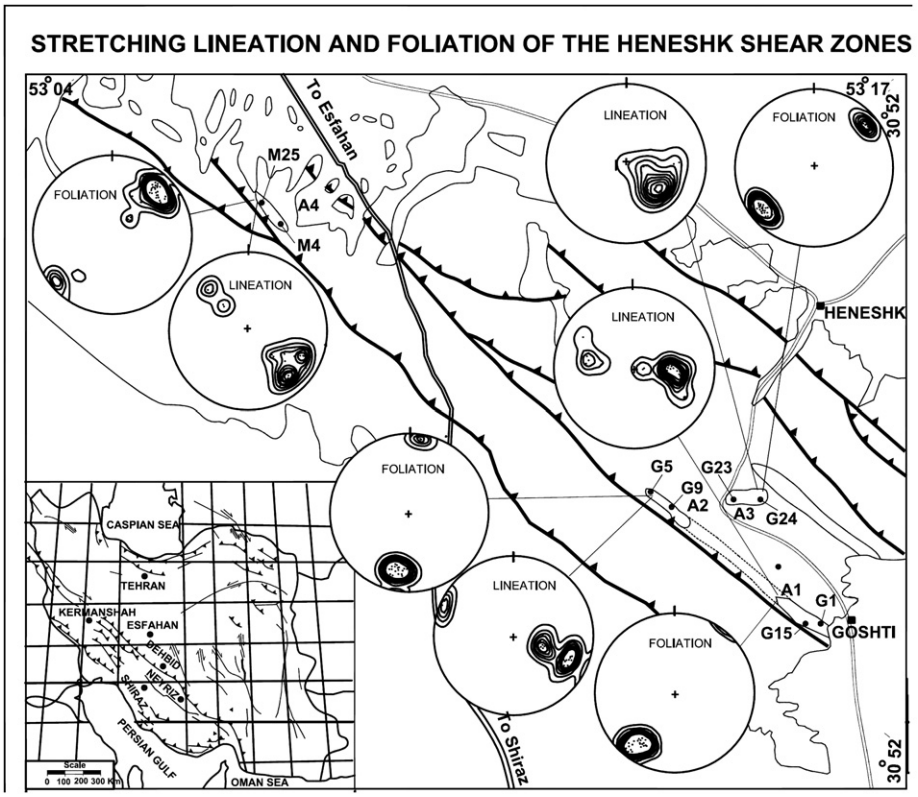

Fig. 7. Generalized structural map of the Goshti area showing the location of A_1, A_2, A_3 and A_4 shear zones outcrops. Field measurements of the foliations (C-plane shear bands of the S/C fabrics), and stretching lineations defined by the long axes of ellipsoidal quartz grains and long narrow quartz ribbons are presented in lower-hemisphere, equal area projections in the four shear zone outcrops.

of quartz ribbons. Its trend varies from S48°E to S65°W with a sub-horizontal (16°) to intermediate (43°) plunge. In A_2, the stretching lineation plunges are shallow and they steepen up progressively in A_3 with a constant trend. In general, the variation is gradual and the mean plunge and trend of all stretching lineations is 43°, S 59° E (Fig. 7). The stretching lineations are parallel to sub-parallel with the strike of the foliations and sometimes significantly oblique or down-dip. The variations of foliation and lineation are similar. Stretching lineations lying almost strike-parallel, or significantly oblique, or approximately down-dip are all feasible in inclined transpression zones, so that the angle of pitch of the lineation within the foliation plane can vary from almost 0° to nearly 90° (Jones et al., 2004). As mentioned before, the thrust sheets are part of the ''Main Zagros Thrust Zone'' of the internal zone. According to Tikoff and Teyssier (1994), once strike-slip and thrust faults are formed, they will continue to be active during deformation because they are well oriented to accommodate the transcurrent and contractional components of deformation. Therefore, it is likely that strike-slip and reverse faults are active simultaneously during orogenic processes.

6. Microstructures

Microscopic examination of oriented thin sections (*XZ*-plane) of the Goshti mylonite indicates that they are composed of quartz, albite, muscovite and biotite (Fig. 8a and b). Quartz porphyroclasts (0.15 to 4.0 mm) are wrapped by fine-grained muscovite and quartz matrix (12–24 μm) forming mantled porphyroclasts. The mantled porphyroclasts show two shear-band cleavages: C-type shear band cleavages (Passchier and Trouw, 2005; Berthe et al., 1979a,b), which are parallel to the shear zone boundary (SZB) and S-type which are at high angles to the C-plane. C-type shear bands form an angle of 30–40° to S-type shear bands. Fine-grained muscovite and quartz around the ellipsoidal quartz porphyroclasts form symmetrical σ-type (Figs. 8a and b) and asymmetrical δ-type mantled porphyroclast systems. The geometry of the σ-type porphyroclast systems indicates a dextral sense of shear.

6.1. ''V'' pull-apart microstructures

The quartz porphyroclasts in the mylonite show varieties of micro-shear zones or micro-faults, which caused displacement of the porphyroclast fragments. Micro-faults make an angle of 30° with the C-type shear band cleavages. Two types of micro-faults are recognized. They include bookshelf structures (Etchecopar, 1977; Ramsay and Hubber, 1987) and pull-apart structures (Hippertt, 1993; Samanta et al., 2002). The bookshelf structures in the porphyroclasts show sets of parallel synthetic slips which are parallel to the regional dextral sense of shear. The fragments of quartz and albite porphyroclasts are separated during rotation and they form ''V'' pull-apart microstructures (Fig. 8c and d).The fracture angle varies from 15° to

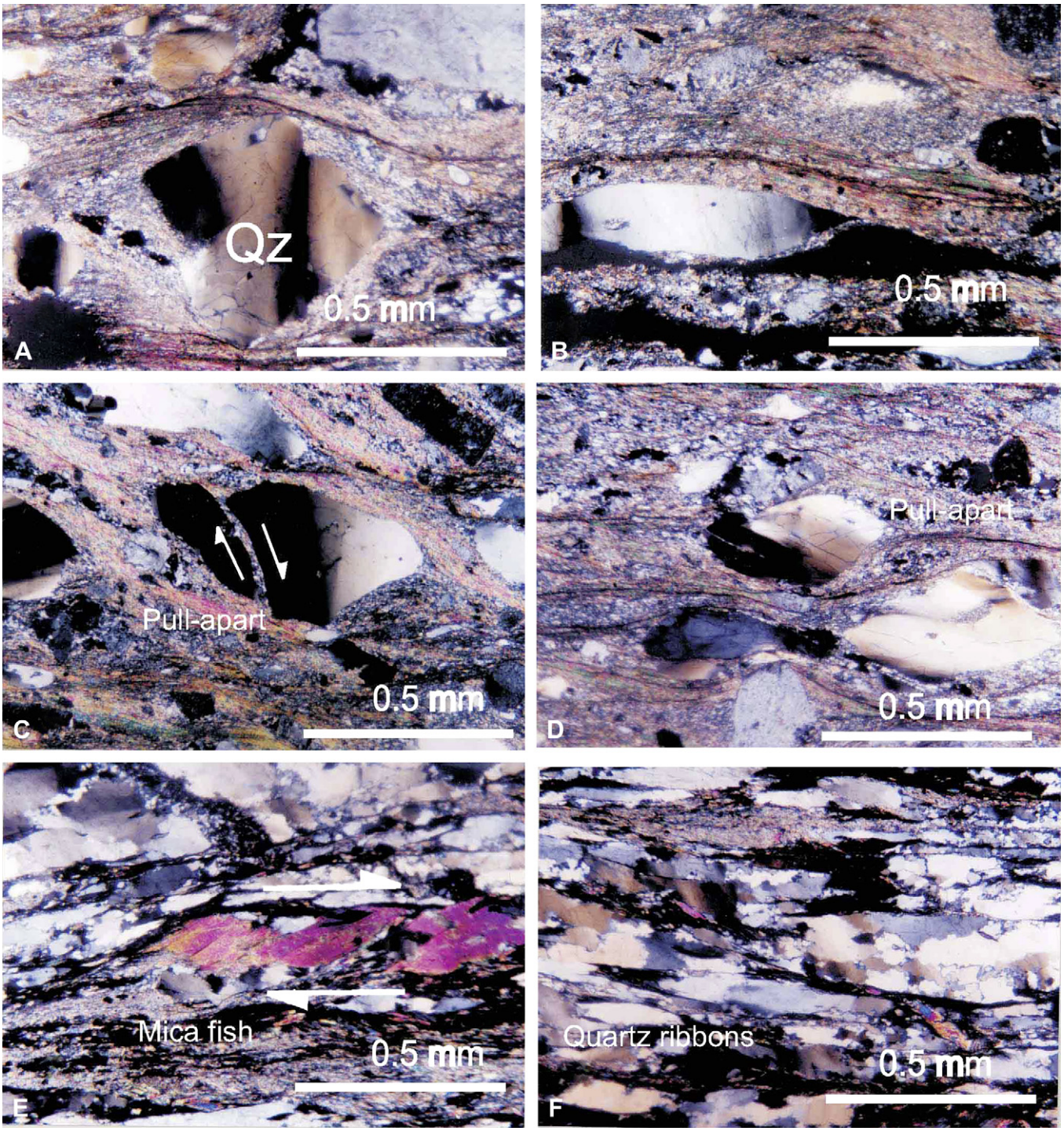

Fig. 8. Optical micrographs showing quartz and mica microstructures. All sections cut perpendicular to the foliation and parallel to the stretching lineation. (A) Typical mantled quartz porphyroclasts wrapped in fine-grained quartz and muscovite, forming σ-type porphyroclast systems. (B) Partially recrystallized quartz ribbon wrapped in fine-grained muscovite and quartz. (C) Quartz porphyroclasts transected by micro-faults and quartz fragments that are separated and rotated forming pull-apart structures. (D, E) Well-developed mica "fish" with monoclinic shape symmetry display a dextral shear sense. The mica "fish" is oblique to the quartz ribbons. (F) Elongated and dynamically recrystallized quartz ribbons in a strongly deformed quartzite boudin.

40°. Two types of "V" pull-apart geometry are recognized. Centrally located fractures produced parallel geometry (type I) pull-aparts and off-centered fracture geometry (type II; Samanta et al., 2002). The "V" pull-apart is filled with fine-grained muscovite which displays a strong preferred orientation.

6.2. Mica "fish"

Well-developed mica "fish" with monoclinic shape asymmetry and curved sides adjacent to the quartz ribbon boundaries are present in the mylonite (Fig. 8e). They show evidence of slip along the (001) cleavage forming listric

micro-faults. The slip along the curved cleavage displays bookshelf structures. The most characteristic micro-structural features of type II S–C mylonites are mica "fish" produced by boudinage and micro-faulting of pre-existing white mica grains (Lister and Snoke, 1984). Some other mica "fish" may be formed from several mica grains in a group. They are surrounded by the dynamically recrystallized matrix and quartz ribbons, forming a δ-type porphyroclast system. The shape of "fish" allows micro-structural assessment of the bulk shear sense, independent of the kinematic indicators (Lister and Snoke, 1984). Mica "fish" geometries are consistent with a dextral shear sense.

6.3. Quartz ribbons

The quartzite ribbon mylonite was collected from strongly deformed quartzite layers and boudins of asymmetrical folds, boudinaged and refolded veins in phyllonite. The phyllonite of the Ghoshti shear zones was cut perpendicular to the foliation (*XZ*-plane) and parallel to the stretching lineation.

The quartz grains are strongly elongated and stretched, forming predominantly quartz ribbons in *XZ* sections (Fig. 8f). The quartz ribbons have aspect ratios from 2:1 to 7:1. Grain boundaries vary from straight to irregular but generally are straight to slightly curved. The ribbons show evidence of internal deformation like undulatory extinction and recrystallization. Recrystallized quartz ribbons in the low to intermediate temperature mylonite show an internal fabric defined by small, elongate grains disposed at angles of 20–45° to the S-plane, which has been referred to as grain shape fabric (GSF) (Burg, 1986). The slightly curved boundaries form an angle of 15–25° to the S-plane.

7. Quartz c-axis fabrics

Oriented samples of quartz–feldspar mylonite, quartz ribbon mylonite, quartzitic mylonite of A_1, A_2, A_3 and A_4 shear zones were collected (Fig. 7; 4113 quartz *c*-axes were measured). Optic *c*-axis measurements were carried out on thin sections cut perpendicular to the foliation plane (*XZ*-plane) and parallel to the stretching lineation using a 5-axis U-stage. C-axes of quartz porphyroclasts, recrystallized quartz and quartz ribbons were measured separately. The *c*-axis orientations were plotted with respect to the mesoscopic foliation framework on equal-area, lower hemisphere stereographic projections and contoured using SpheriStat software to obtain the fabric diagrams presented in Fig. 9.

Measurements of quartz porphyroclast *c*-axes of samples G_{12} and G_{15} from the A_1 Station (Figs. 7 and 9) southwest of the Goshti village indicate that the LPO patterns (Fig. 9) display slight external asymmetry (Behrmann and Platt, 1982; Platt and Behrmann, 1986), defined by the angle of obliquity (ψ) between the central segment of the fabric skeleton and the foliation plane (Fig. 10; Law, 1990). The ψ angles for the G_{12} and G_{15} samples are 70° and 80°. The quartz *c*-axis asymmetry and single-girdle relative to the foliation plane indicate non-coaxial progressive deformation. Quartz *c*-axis maxima aligned parallel to the inferred intermediate principal strain direction (*Y*-axis) have commonly been interpreted as indicating that prism <a> is the dominant slip system (Wilson, 1975; Bouchez, 1977; Lister and Dornsiepen, 1982).

Measurements of quartz porphyroclast *c*-axes for the G_5 and G_9 samples from the A2 station were carried out. The A_2 station is part of the Goshti shear zone and it is possibly a continuation of the A_1 station (Fig. 7). These two samples are similar to G_{12} and G_{15} and they have strongly developed single-girdle fabrics relative to the foliation plane (Fig. 9). The G_5 sample shows evidence of a transition from point maxima crossed-girdle fabrics to single-girdle point maxima fabrics. At low temperature, basal <a> is the most important slip system and girdles may have a strong cluster of *c*-axes at their periphery. With increasing temperature, prism <a> slip becomes more important and the girdle tends to a maximum around the *Y*-axis (Wilson, 1975; Bouchez, 1977; Lister and Dornsiepen, 1982; Law, 1990). The angle of obliquity (ψ) between the central segments of the fabric to the foliation plane is 66° and 73°, respectively. Both central segments are slightly asymmetric relative to the foliation plane and point maxima are at low angles to the *Z*-axis (20° and 24°). Sample G_5 is characterized by an external asymmetry (ψ) and internal asymmetry (ω_1 and ω_2) as suggested by Law (1990). The trailing edges of *c*-axis fabric skeletons show angles of 54° and 40°, respectively. The external and internal asymmetry of fabrics indicates a dextral sense of shear (Fig. 9).

c-Axis fabric skeletons for the quartz porphyroclasts (G_{23} and G_{24} samples) are associated with the A_3 shear zone (Figs. 7 and 9), northeast of the Goshti village, and display a type-I crossed-girdle pattern. Both *c*-axis fabric skeletons show external and internal fabric asymmetry ($\psi = 80°$, $\omega 1 = 30°$ and $\omega 2 = 56°$ for G_{23} sample). The internal and external asymmetries of fabrics indicate a dextral shear sense (Fig. 9). The type I crossed-girdle pattern can be explained as an effect of the activity of basal <a> slip and rhomb <a> slip (Passchier and Trouw, 2005). At low-metamorphic grade conditions (300–400 °C) intracrystalline slip of quartz occurs preferentially on basal <a> system (Bouchez, 1977).

7.1. Quartz ribbon c-axis fabrics

C-axis fabric from the A_4 station (samples M_4 and M_{25}) are mainly measured from quartz ribbons and recrystallized quartz grains. Quartz ribbons display a well-developed lattice preferred orientation (LPO). The fabric skeletons show strongly developed single girdles (Fig. 9), slightly asymmetric relative to the foliation plane ($\psi = 85°$ for M_4 sample and $\psi = 66°$ for M_{25} sample). The maxima are located between the *Y*- and *Z*-axes of the strain ellipsoid, which is commonly interpreted to indicate rhomb <a> as the dominant slip system (Wilson, 1975; Bouchez, 1977; Lister and Dornsiepen, 1982; Law, 1990).

The *c*-axis fabrics of recrystallized grains in the same samples (M_4 and M_{25}) are somewhat different from those of the quartz ribbons; they have a strong asymmetry and a smaller angle to the foliation plane ($\psi = 55°$ to 58°). Also in some

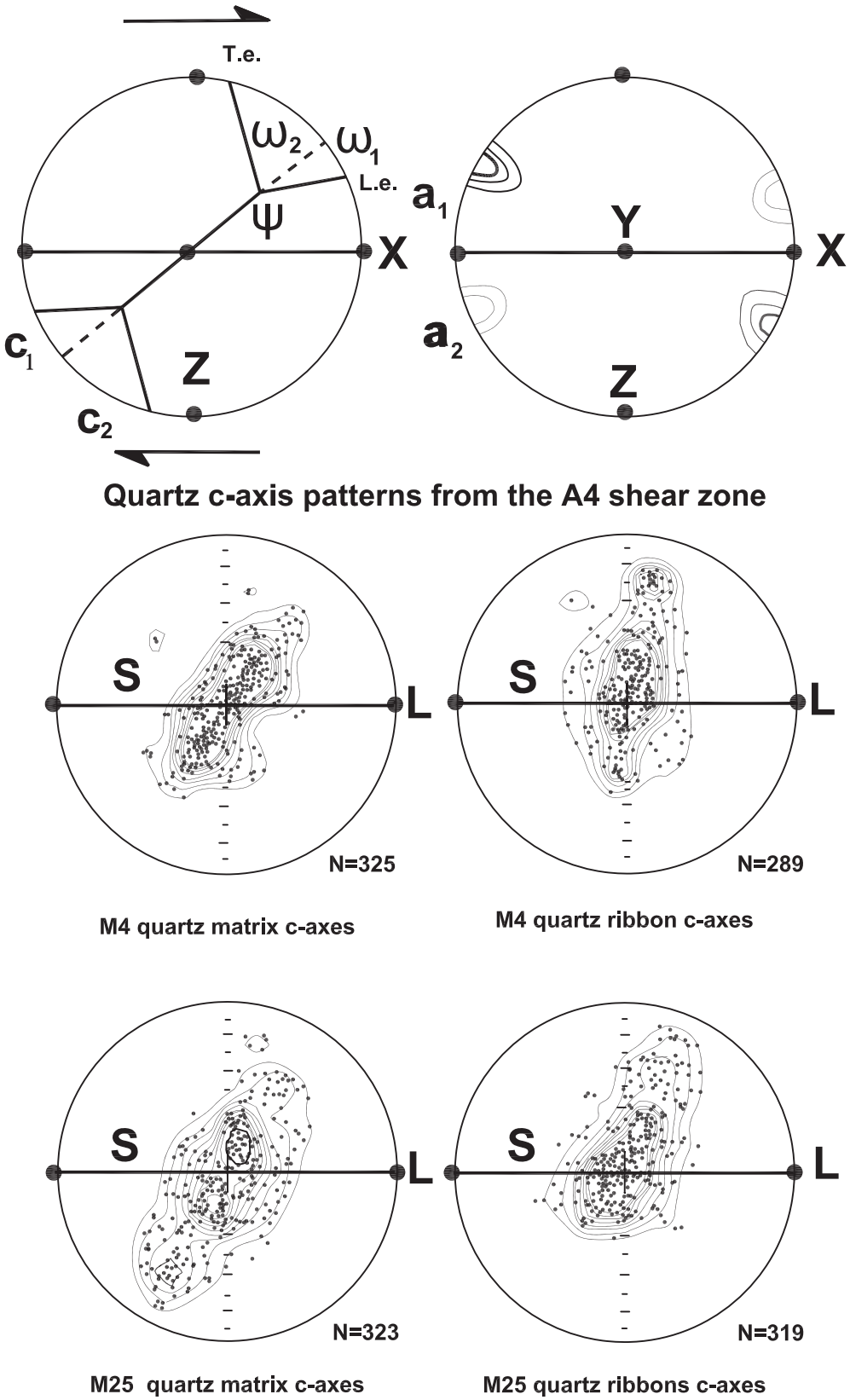

Fig. 9. Quartz *c*-axis fabric measurements from the A_1, A_2, A_3 and A_4 Goshti shear zones (locations shown on Fig. 7). Parameters used to characterize external and internal fabric asymmetry in quartz *c*- and *a*-axis fabrics (Law, 1990) include external fabric asymmetry (characterized by ψ, c_1, c_2, a_1 and a_2), internal fabric asymmetry (characterized by ω_1 and ω_2). Dextral shear sense indicated by the unequal densities of *a*-axis point maxima and asymmetry of the *c*-axis fabric skeleton and *a*-axis point maxima. Leading and trailing edges of the *c*-axis fabric skeleton are denoted by l.e and t.e, respectively.

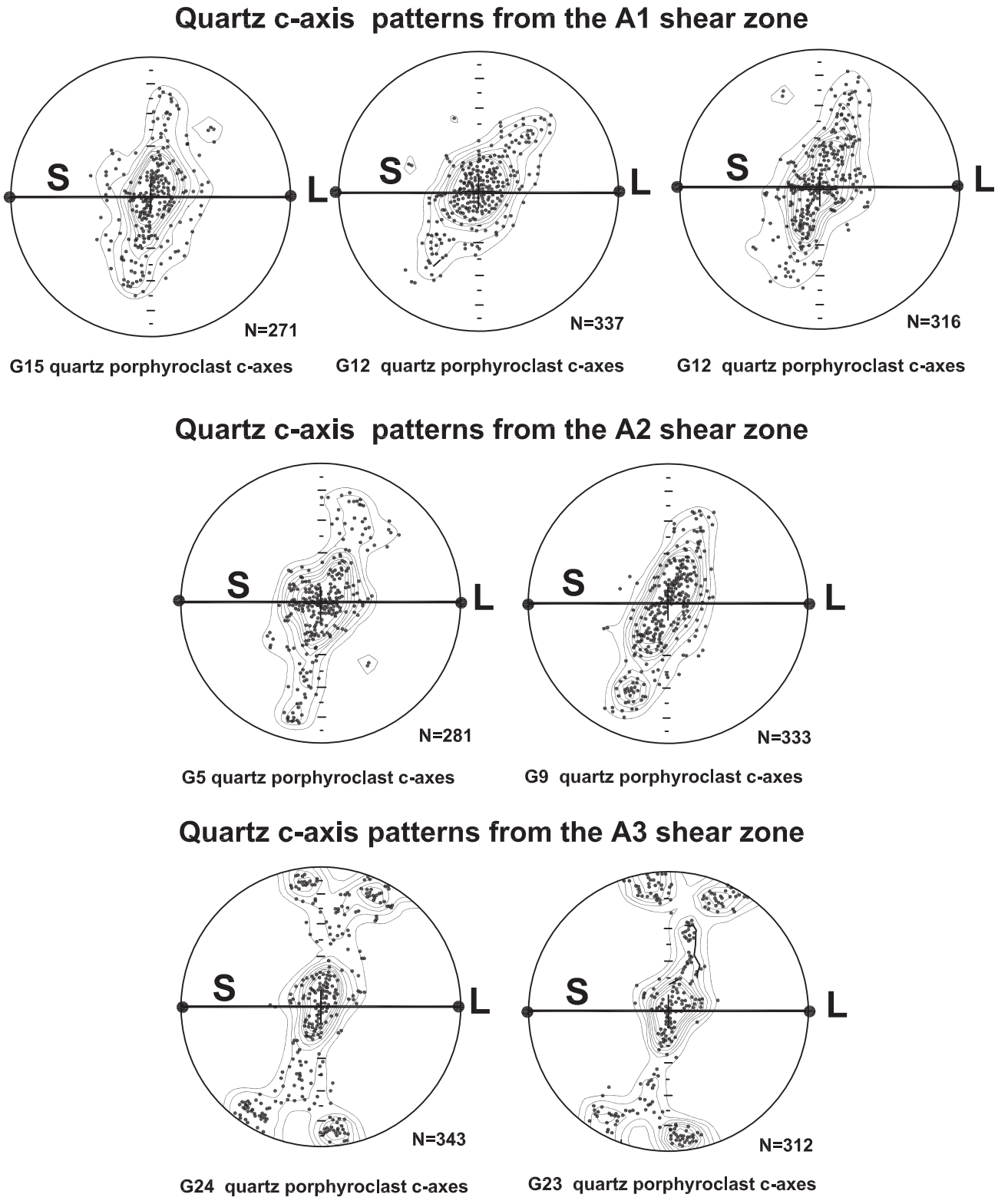

Fig. 9 (*continued*).

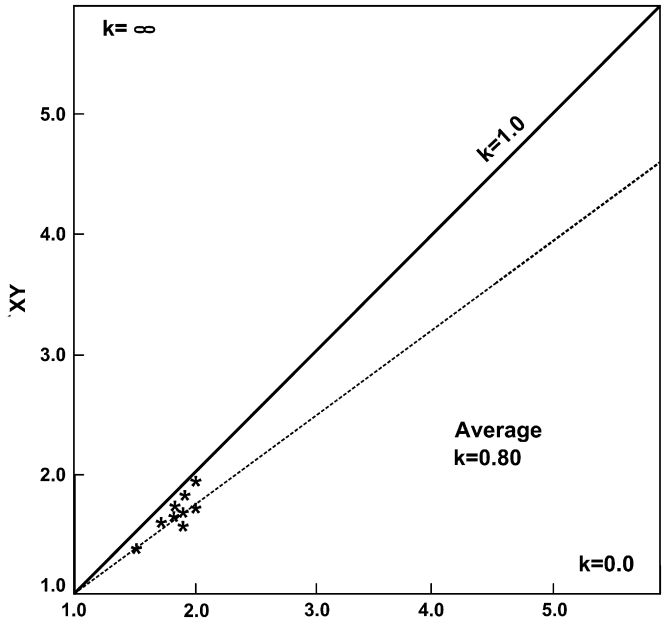

Fig. 10. Geometric means of R_{XY} against mean of R_{YZ} of the quartz porphyroclasts are plotted for each sample on the Flinn diagram (Flinn, 1962). The field of plotted porphyroclasts shows k-values = 0.80, which is characteristics of an oblate triaxial ellipsoid.

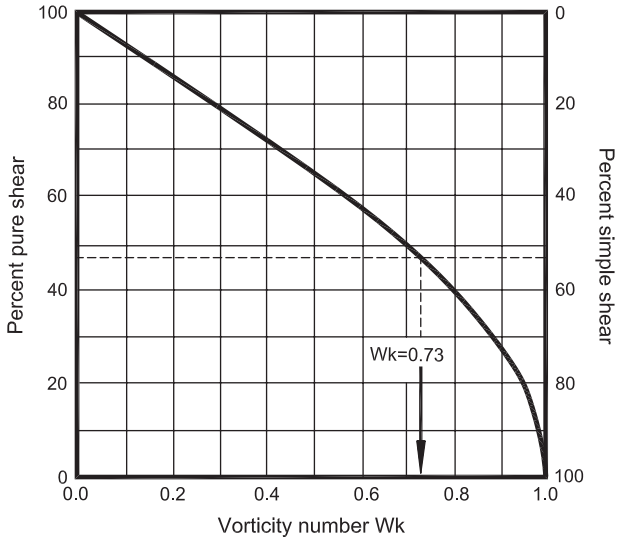

Fig. 11. Relation between kinematic vorticity number W_k and components of pure and simple shear for instantaneous 2D flow; pure shear and simple shear components make equal contributions to flow at $W_k = 0.71$ (Law et al., 2004). The mean estimated $W_k = 0.73$ (arrow) shows that 47% pure shear and 53% simple shear contributed to flow apophysis. $W_k = \cos\alpha$, where α is the angle between flow apophysis (Bobyarchick, 1986) and varies from 0° (simple shear) to 90° (pure shear). The relative proportion of pure shear to simple shear is given by $\alpha/90°$; at $\alpha = 45°$ there should be equal contributions (45°/90° = 0.5) (Law et al., 2004).

samples, there is a c-axis maximum at the Y-axis. This external asymmetry of the fabric indicates a dextral shear sense.

8. Strain analysis

8.1. Finite strain method using the mathematical means of the quartz porphyroclasts

Ten oriented samples of quartz–feldspar porphyroclastic mylonite (2.0 mm to 4.0 mm quartz grain size) from thick lithological domains were selected for strain and vorticity analysis throughout the A_1 and A_2 shear zones (Fig. 7). Each oriented sample was cut on three orthogonal sections, one cut parallel to the foliation plane (XY), and the other two perpendiculars to the foliation and to each other (YZ), with one section (XZ) cut parallel to the stretching lineation. The outline of each quartz porphyroclast was marked on tracing paper from microscopic photomicrographs and its long (X), intermediate (Y), and short (Z) axes measured. Then the aspect ratios (R_f) X/Y, X/Z and Y/Z were calculated. The geometric mean (G) and harmonic mean (H) of the X/Y, Y/Z and X/Z axial ratios were calculated according to method of Ramsay and Hubber (1983). The calculated geometric mean for three perpendicular sections axial ratios shows values of $R_S = 2.30 \pm 0.82$ for the XZ sections. The calculated geometric mean values for the XY section is $R_S = 1.93 \pm 0.46$. Lisle (1979) concluded that the harmonic mean of all R_S values is closest to the real applied strain.

The geometric means of R_{XY} against the means of R_{YZ} are plotted for each sample on a Flinn diagram (Flinn, 1962), indicating a deformation field near $k = 0.80$ (Fig. 11). The position is characteristic for an oblate triaxial ellipsoid ($s_1 > s_2 > s_3$).

8.2. Shear strain

The shear strain was estimated from the geometry of the quartz c-axis fabric asymmetry (Fig. 9) of central girdle segments (Fig. 9; $90° - \psi$) relative to the foliation plane (XY-plane). The shear strain (γ) and β angle generally obey the relationship of Ramsay's law of $\gamma = \tan\beta$ at large scale. The estimated shear strain γ varies from 0.18 to 0.84. There are variations in the porphyroclast c-axis fabrics, relative to the dynamically recrystallized c-axis fabrics; the latter show higher shear strain.

9. Kinematic vorticity analysis

9.1. Method I. Rotated porphyroclasts

A measure of the orientation and aspect ratios of relatively rigid objects (e. g. porphyroclasts/blasts) rotating in a homogeneous deformed matrix can provide an estimate of W_k (Passchier, 1987; Simpson and De Paor, 1997; Wallis et al., 1993). This method is based on the theoretical work of Jeffrey (1922), Ghosh and Ramberg (1976) and Passchier (1987) who describe the mobility of rigid particles in a steady state non-coaxial flow regime. Critical prerequisites for applying this analysis are reasonably homogeneous deformation at the microscopic scale and a relatively large number of particles.

Six quartz-rich samples (G_1 to G_6), which contain abundant quartz porphyroclasts, were analyzed by measuring the angle between the long axes of porphyroclasts with the mesoscopic foliation and different aspect ratios of the long and short axis. According to Passchier and Trouw (2005), the value of the critical aspect ratio, Rc, at which clasts rotate freely and develop δ-type mantles, is a function of W_k:

$$W_k = \left(Rc^2 + 1\right)\left(Rc^2 - 1\right) \quad (1)$$

The calculated W_k is the range of 0.41 to 0.95.The estimated mean W_k is 0.75 ± 0.23.

9.2. Method II. Quartz c-axis fabrics and strain ratio

According to Wallis (1992) and Wallis et al. (1993), the angle β between the perpendicular to the central girdle of a quartz c-axis diagram and the foliation is equal to the angle between the flow plane and the principal plane of strain. It is assumed that there is no dynamic recrystallization, which can continuously "re-set" the LPO (personal communication, J. Tullis). The angle β is a function of R_{XZ} (strain ratio and W_k, as expressed by:

$$W_k = \sin\left\{\tan^{-1}\left[\frac{\sin(2\beta)}{[(R_{XZ}+1)/(R_{XZ}-1)] - \cos(2\beta)}\right]\right\} \times \frac{(R_{XZ}+1)}{(R_{XZ}-1)} \quad (2)$$

The calculated W_k-values range from 0.34 to 0.94. The estimated mean W_k is 0.72 ± 0.25. The agreement between method I and method II gives more confidence in the results. The estimated mean W_k from the two methods is 0.73 ± 0.02.

10. Discussion

10.1. .Zagros Thrust System

The Goshti shear zones and Heneshk duplex structures are part of the Zagros Thrust System of the hinterland zone of the Zagros orogenic Belt. The Zagros Thrust System in this area consists of eight sheets of NW-striking (N30°W to N45°W), NE-dipping dextral strike-slip duplex structures that are linked with imbricate fans and oblique slip thrusts. The Zagros Thrust System was previously considered to be a "Crush Zone" (Wells, 1969), or the "Main Zagros Thrust Zone" (Takin, 1972; Hynes and McQuillan, 1974; Berberian and King, 1981; Berberian et al., 1982), or the "Main Zagros Reverse" or the "Suture Zone" (Berberian, 1995). The so-called "Main Zagros Thrust" which is traditionally considered as the boundary between the Sanandaj–Sirjan Zone and the Zagros Simply Folded Belt is by no means a single "high-angle reverse fault", nor is it a narrow zone of "crush rocks" (Alavi, 1994). The thrust system is an array of kinematically, geometrically and mechanically related faults that developed in a sequence during regional deformation and are associated with deformation above a basal detachment (Boyer and Elliot, 1982; McClay, 1992). Therefore it is more reasonable to classify and name it as the Zagros Thrust System (Fig. 13) rather than the "Main Zagros Thrust Zone" or "high-angle reverse fault" or "Crush Zone". The Zagros Thrust System with various components of dextral strike-slip, imbricate fans, oblique slip thrusts, shear zones and brittle listric faults contains elements that are consistent with inclined transpression, including components of strike-slip and dip-slip (Jones et al., 2004). In addition, the Zagros Thrust System has significant components of dextral shear along the thrust sheets, in which variation in the quartz c-axis fabric asymmetries can be related to a high proportion of simple shear (non-coaxial) relative to pure shear (coaxial) deformation (Figs. 10 and 11).

10.2. Simple-shear and pure-shear components of deformation

The Goshti shear zones are the sole thrusts or basal decollement planes of the Zagros Detachment Zones (Fig. 13). The shear zones contain symmetrical σ-type and asymmetrical δ-type mantled quartz porphyroclasts. The quartz porphyroclasts were used to estimate the kinematic vorticity number (Ghosh and Ramberg, 1976; Passchier, 1987). For plane-strain deformation, components of pure shear and simple shear can be related in terms of the kinematic vorticity number W_k (Means et al., 1980).

The estimated kinematic vorticity number of $W_k = 0.73$ can be considered as instantaneous deformation (W_k), rather than finite deformation (W_m). W_k (instantaneous deformation) is equal to W_m (finite deformation) in steady-state deformation (Law et al., 2004). In non-steady-state deformation, flow is

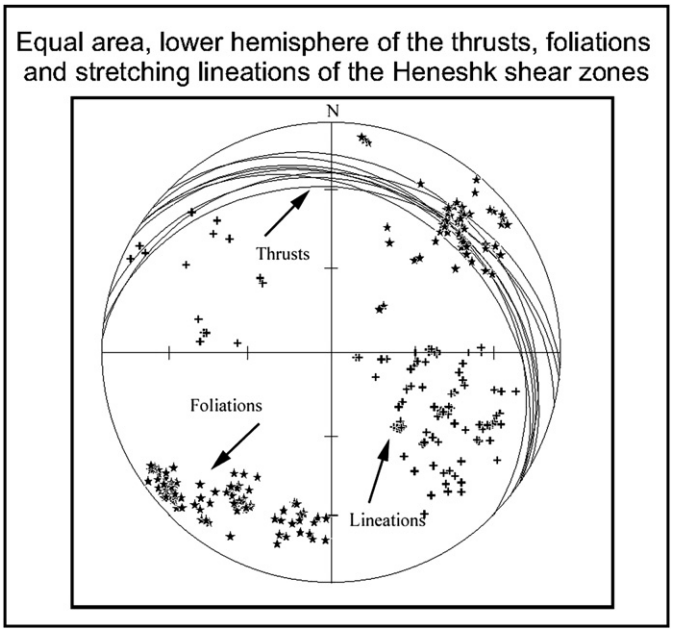

Fig. 12. Equal area, lower-hemisphere stereographic projection of the poles to foliation and stretching lineation for the Heneshk shear zones. Great circles represent the orientations of the shear zones and thrusts. In the shear zones, both foliation and lineation are well developed. The orientation of lineations defined by elongated quartz porphyroclasts changes progressively from sub-horizontal to sub-vertical.

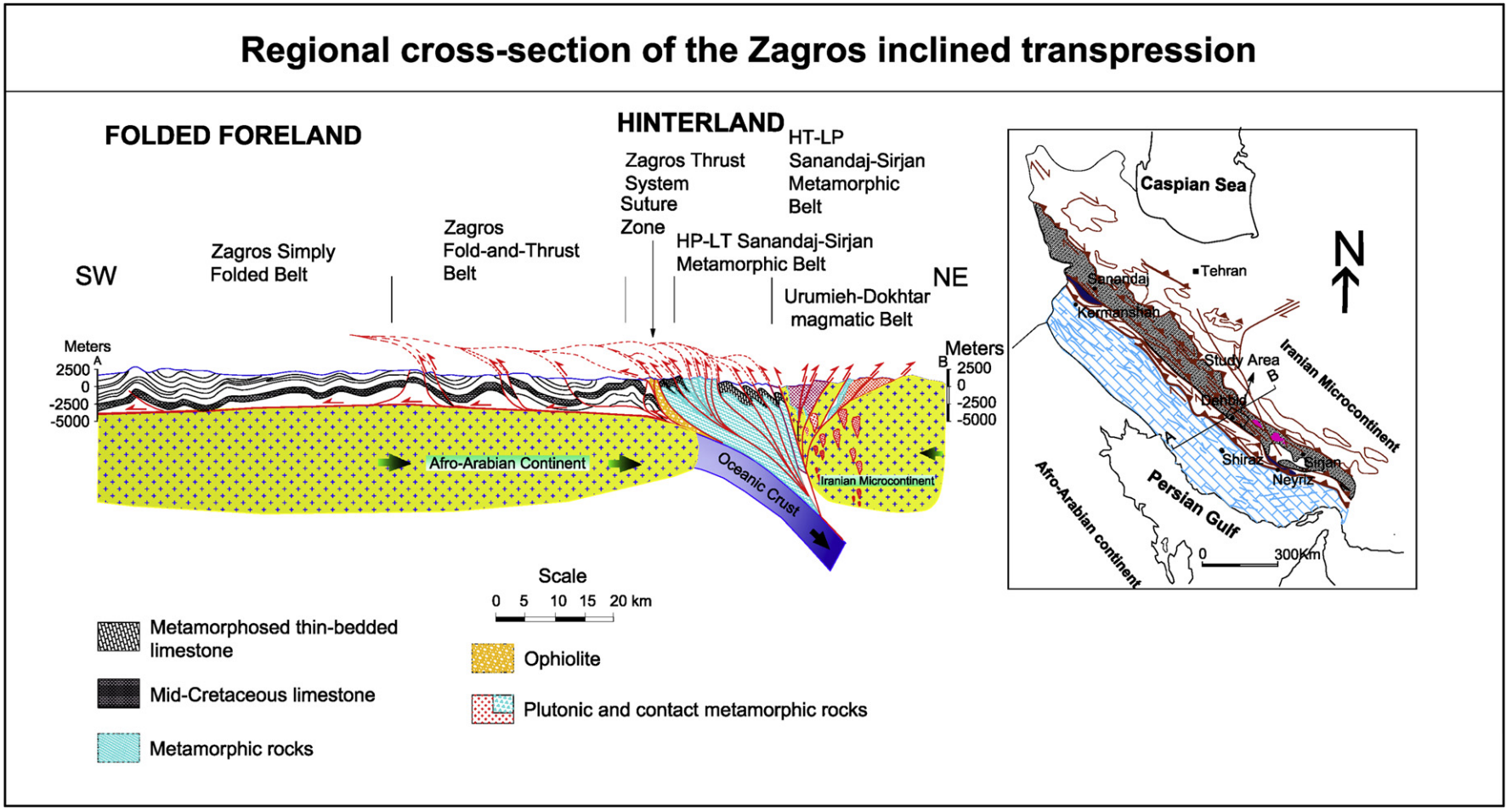

Fig. 13. Large-scale regional cross section of the Zagros inclined transpression from southwest to northeast (A to B section), showing: (1) Zagros Simply Folded Belt; (2) Zagros Fold-and-Thrust Belt (Stöcklin, 1968; Berberian and King, 1981; Alavi, 1994); (3) Zagros Thrust System; (4) Zagros Suture Zone/Ophiolite Zone (Sarkarinejad, 2005); (5) HP-LT/HT-LP Sanandaj–Sirjan paired metamorphic belts, (Sarkarinejad, 1999,); (6) Urumieh–Dokhtar Magmatic Belt.

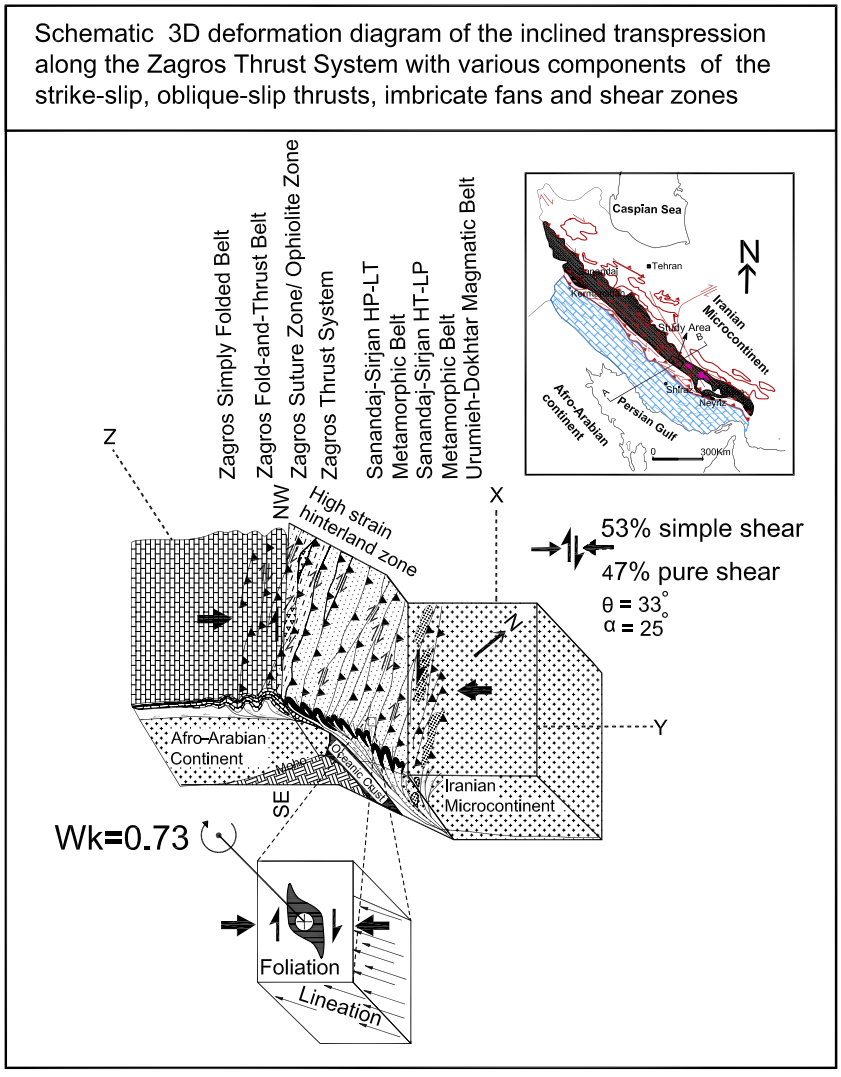

Fig. 14. Block diagram showing the 3D geometry of the Afro-Arabian continent and Iranian micro-continent with an inclined transpression zone along the Zagros Thrust System. The maximum incremental axis angle is 33°. The angle α of the inclined plate convergence or direction of flow apophysis is 25° and the mean kinematic vorticity number $W_k = 0.73$. The model predicts 40% strike-slip partitioning.

more appropriately characterized by the mean kinematic vorticity number W_k in which flow is integrated over space and time (Passchier, 1988). The estimated mean finite deformation (W_m) value indicates 47% pure shear component and 53% simple shear component of deformation (corresponding to $W_k = W_m = 0.73$; Fig. 11). Components of simple shear and pure shear deformation were involved in the formation of strike-slip, oblique-slip and NE–SW compression of the Zagros inclined transpression.

10.3. Inclined dextral transpression

The structural and kinematic characteristics of inclined dextral transpression of the Zagros Orogenic Belt include a systematic variation in the plunges of the shallow to intermediate stretching lineation (Fig. 12), S–C fabric components and asymmetrical structures of bulk transpressional deformation, regionally consistent dextral shear sense, and obliquity partitioning of $k < 1$ as oblate triaxial ellipsoids ($s_1 > s_2 > s_3$) (Figs. 10 and 12). The kinematic vorticity number W_k (instantaneous deformation) also confirms characteristics of a transpressional zone (Fig. 14).

The angle θ between the minimum instantaneous strain axis (ISA) s_3 and the transpressional zone boundary corresponds to a unique W_k (Fossen and Tikoff, 1993). The calculated kinematic vorticity number (W_k) based on the quartz c-axis and rotated porphyroclasts methods is $W_k = 0.73$. Using this W_k value, the estimated θ angle is 33°. According to Fossen and Tikoff (1993) in pure-shear dominated transpression $0.81 > W_k > 0$ and $0° \leq \theta \leq 35°$, s_1 and s_3 lie in a vertical plane and a reverse fault should form (Tikoff and Teyssier, 1994). Applying the relationship between the θ angle of the maximum horizontal axis of incremental strain ellipsoid with the plate margin and the angle α (Tikoff and Teyssier, 1994), which is the angle of plate convergence or the direction of the contractional apophysis, the estimated α angle of plate convergence between the Iranian micro-continent and the Afro-Arabian continent is 25° (Fig. 14).

According to the NUVEL-1A estimates, which is based on the analysis of global sea-floor spreading, fault systems and earthquake slip vectors, the Arabian plate is moving N13°E at a rate of about 31 mm yr^{-1} relative to Eurasia at the longitude of 52°E (DeMets et al., 1990, 1994). GPS measurements indicate that northward motion of the Arabian plate relative to Eurasia is slower than the NUVEL-1A estimates (e.g. 22 mm yr at N8° ± 5°E; Vernant et al., 2004). Recent GPS surveys indicate that Zagros kinematics correspond to an oblique convergence between the rigid central Iranian plateau and the Arabian plate of ~7 mm yr^{-1} at the longitude of the Persian Gulf. Convergence is almost frontal in the SE Zagros and oblique (45°) in the NW part of the Zagros (Vernant and Chery, 2006).

Given the presence of dextral shear sense indicators such as S–C fabrics, mica ''fish'', pull-apart structures, and quartz porphyroclast *c*-axis skeletons, the interpretation is that the Zagros Thrust System in the Heneshk area is a dextral transpressional shear zone (Fig. 14). Using the angle of plate convergence as a flow apophysis of the displacement field within the inclined transpressional zone ($\alpha = 25°$), the predicted direction of the maximum vertical axis of the instantaneous strain ellipsoid (ISA) is about $\theta = 33°$ from the orientation of the shear zone (Fig. 14). The θ angle correlates well with the field measurements of the stretching lineations of fold axial planes which lie in the range from shallow to intermediate plunges relative to the trends of the Heneshk dextral shear zones. These stretching lineations reflect the instantaneous strain axes. According to Tikoff and Teyssier (1994), the partitioning of the strike-slip component of oblique convergence results in the re-orientation of the instantaneous strain axes (ISA) within the distributed deformation zone, forming an angle (θ) relative to the deformation margin. Increasing the strain partitioning within such a system results in a decrease in θ. This implies that about 40% of strike-slip deformation is required to accommodate the finite strain and the re-orientation of instantaneous strain axes.

The finite strain determined from the harmonic mean calculations from porphyroclasts in *XZ* sections yields values of $R_S = 2.30$. Plotting the geometric mean of R_{XY} against the geometric mean of R_{YZ} in a Flinn (1962) deformation diagram gives a deformation field at $k = 0.80$, indicating an oblate triaxial ellipsoid ($0 < k < 1$). Liu et al. (1995) defined a parameter k to measure the degree of obliquity partitioning; $k = 0$ and $k = 1$ are two end member cases of no obliquity and complete obliquity partitioning. Our value of $k = 0.80$ displays intermediate obliquity partitioning.

10.4. Zagros Thrust System deformation phases

The Sanandaj–Sirjan HP-LT metamorphic belt and Zagros Thrust System exhibit three distinct deformation phases. The first phase of deformation (D1) led to the formation of the main foliation (S1). This NW–SE foliation is parallel to the Zagros Thrust System. The S1 foliation may have formed at the peak of metamorphism, whereas later events (S2) are characterized by deformation of this foliation to produce weaker and less penetrative foliation under lower grade or drier metamorphic conditions (Passchier and Trouw, 2005). The third phase of deformation (D3) developed by shear along the shear zones and thrusts and gave rise to the S/C shear band cleavages (S3).

Based on all geochronological ages (Hynes and Reynolds, 1980; Sheikholeslami et al., 2003), it can be suggested that the S1 foliation was synchronous with the peak of metamorphism and is related to the inclined collision of the Afro-Arabian and Iranian micro-continents from the Middle Jurassic to the Early Aptian. Further inclined collision of the Zagros Thrust System and oblique-slip extrusion of the high-grade metamorphic rocks related to the most deeply subducted materials on top of the NE-dipping subduction zone occurred during Albian to Campanian time. Inclined extrusion of the high-grade metamorphic rocks (such as eclogite, amphibolite and kyanite schist) produced an accretionary prism and wedge-shaped Sanandaj–Sirjan HP-LT metamorphic belt (Figs. 13 and 14). Extrusion of the deep-seated Zagros sole thrusts or detachment-shear zones along the Zagros Thrust System, with both simple-shear and pure shear components, also related to this event.

10.5. Geometric relationships between quartz c-axis pattern and stretching lineation

Measurements of the *c*-axes of quartz porphyroclasts and ribbons show two types of patterns. The quartz porphyroclasts and ribbons from the A_1, $A_2$and A_4 shear zones along the Zagros Thrust System have strongly developed asymmetrical single girdle patterns. Quartz porphyroclast *c*-axes measurements in the A_3 shear zone developed type I crossed girdle patterns, asymmetric to the foliation plane. Quartz *c*-axes in a single girdle pattern have point maxima concentrated around the *Y*-axis. In the type I crossed girdle patterns, quartz *c*-axes are concentrated between the *Z*- and *Y*-axes. The G_5 sample from the A_2 shear zone shows evidence of a transition from a type I crossed girdle to a single girdle pattern. Heilbronner and Tullis (2006) showed that a progressive transition occurs from *Z*-axis to *Y*-axis maxima with increasing strain-induced grain boundary migration recrystallization. Such a change from a type I crossed girdle to a single girdle pattern. in pattern can also result from an increase of deformation temperature. The presence of a single girdle pattern in which *c*-axis point maxima concentrate around the *Y*-axis indicates that deformation occurred under amphibolite conditions (Schmid and Casey, 1986). The presence of *Y*-axis maxima implies that only <a> slip was active in quartz during deformation, suggesting no [c] slip, which indicates that the temperature of deformation did not exceed 650 °C (Passchier and Trouw, 2005) or 500 °C (Okudaira et al., 1995). The *c*-axis patterns thus indicate that quartz deformed under epidote-amphibolite facies conditions (Hietanen, 1967). This means that deformation on the Zagros Detachment Thrusts occurred at a depth of about 20–25 km.

Stretching lineations associated with the shear zones show constant SE-trends but plunges varying from shallow (16–20°) in the A_2 and A_4 shear zones to intermediate (43–55°) in the A_3 shear zone. Shallow plunges are associated with asymmetrical single girdle pattern, whilst intermediate plunges are

associated with the type I crossed girdle. None of these shear zones show evidence of steeply plunging stretching lineations.

Based on the finite strain data from different areas with different lithologies, Sarkarinejad (2007) showed that there is no correlation between magnitude of strain and obliquity of stretching lineation. The obliquity of lineation is controlled primarily by extrusion direction (Czeck and Hudleston, 2004). The obliquity of lineation is mostly controlled by the angle of the nonvertical extrusion direction along the thrust wedge, not the magnitude of the strain or simple- or pure-shear components. Intermediate values of plunge are associated with strains that are recognizably triclinic (Jones et al., 2004). Strain matrix modeling shows that all three axes of the finite strain ellipsoid are non-parallel to the Cartesian reference frame, and they experience complex non-planar rotations during ongoing deformation (Jones et al., 2004). Therefore, it can be concluded that the Zagros Thrust System formed during triclinic dextral transpression in an inclined, obliquely convergent thrust wedge.

11. Summary and conclusions

The Heneshk shear zones are part of the NW-striking, NE-dipping dextral strike-slip Zagros Thrust System of the Zagros orogenic belt. In this portion of the orogenic belt, plastic deformation dominates, and penetrative strain developed. The Zagros Thrust System in this area consists of eight sheets of NW-striking, NE-dipping dextral strike-slip duplex structures that are linked with imbricate fans and oblique slip thrusts.

Using kinematic vorticity number W_k-values, the θ angle between the maximum instantaneous strain axis (ISA) and the transpressional boundary is 33°. Applying the relationship between the θ angle and the plate margin, the estimated angle α of the inclined plate convergence between the Iranian microcontinent and the Afro-Arabian continent is 25°. The presence of dextral shear sense indicators suggests that the Zagros Thrust System formed during triclinic dextral transpression in an inclined, obliquely convergent thrust wedge. In this simple shear and pure shear dominated transpression, about 40% strike-slip partitioning (Fig. 14) is required to accommodate the finite strain and re-orientation of instantaneous strain axes.

Acknowledgements

The authors wish to thank Professor Carlo Doglioni who critically reviewed the manuscript and made valuable suggestions for its improvement. We are grateful to Professor Jan Tullis for critical reading of the manuscript, which greatly improved the presentation, Professor Herb Helmstaedt is thanked for comments and suggestions on an earlier version of the manuscript. Thanks also to Professor Jao Hippertt for a constructive review and editorial comments. Professor Egydio-Silva and Dr. Luis Fernando Grafulha Morales provided thorough reviews that have greatly improved the quality of the final version. Thanks to Ali Faghih for his help. This research was supported by a Shiraz University Research Council (SURC) grant which is gratefully acknowledged.

References

Alavi, M., 1994. Tectonics of the Zagros orogenic belt of Iran: new data and interpretations. Tectonophysics 229, 211–238.

Authemayou, C., Chardon, D., Bellier, O., Malekzadeh, Z., 2006. Late Cenozoic partitioning of oblique convergence in the Zagros fold-and -thrust belt (Iran). Tectonics 25, TC3002, doi:10.1029/200TC1860. 2006.

Berberian, M., 1995. Master "blind" thrust faults hidden under the Zagros folds: active basement tectonics and surface morphotectonics. Tectonophysics 241, 193–224.

Berberian, M., King, G.C.P., 1981. Towards a paleogeography and tectonic evolution of Iran. Canadian Journal of Earth Sciences 12, 210–265.

Berberian, M., Yeats, R., 2001. Contribution of archaeological data to studies of earthquake history. Geology 23, 563–584.

Berberian, M., Muir, I.D., Pankhurst, R.J., Berberian, M., 1982. Late Cretaceous and early Miocene Andean-type plutonic activity in northern Makran and central Iran. Journal of Geological Society London 139, 605–614.

Behrmann, J.H., Platt, J.P., 1982. Sense of nappe emplacement from quartz *c*-axis fabrics: an example from Betic Cordilleras (Spain). Earth and Planetary Science Letters 59, 208–215.

Berthe, D., Choukroune, P., Jegouzo, P., 1979a. Orthogneiss, mylonite and non-coaxial deformation of granites: the example of south Armoricain shear zone. Journal of Structural Geology 1, 31–42.

Berthe, D., Choukroune, P., Gapais, D., 1979b. Orientations Préférentielles de quartz et orthogneissification progressive en régime cisaillant: l'exemple du cisaillement sub-Armorician. Bulletin Minéral 102, 265–272.

Bobyarchick, A.R., 1986. The eigenvalues of steady-state flow in Mohr space. Tectonophysics 122, 35–51.

Bouchez, J.L., 1977. Plastic deformation of quartzites at low temperature in an area of natural strain gradient. Tectonophysics 39, 25–50.

Bowler, S., 1987. Duplex geometry: An example from the Moine Thrust belt. Tectonophysics 137, 25–35.

Boyer, S.E., Elliot, D., 1982. Thrust systems. American Association of Petroleum Geologists Bulletin 66, 1196–1230.

Burg, J.P., 1986. Quartz shape fabric variations and *c*-axis fabrics in a ribbon-mylonite: arguments for an oscillating foliation. Journal of Structural Geology 8, 123–131.

Czeck, D.M., Hudleston, P.J., 2004. Physical experiments of vertical transpression with localized nonvertical extrusion. Journal of Structural Geology 26, 573–581.

DeMets, C., Gordon, R.G., Argus, D.F., Stein, S., 1990. Current plate motions. International Journal of Geophysics 101, 425–478.

DeMets, C., Gordon, R.G., Argus, D.F., Stein, S., 1994. Effects of recent revisions to geomagnetic reversal time scale or estimates of current plate motions. Geophysical Research Letters 21, 2191–2194.

Dutton, B.J., 1997. Finite strain in transpression zones with no boundary slip. Journal of Structural Geology 19, 1186–1200.

Etchecopar, A., 1977. A plane model of progressive deformation in polycrystalline aggregate. Tectonophysics 39, 121–139.

Flinn, D., 1962. On folding during three dimensional progressive deformations. Quaternary Journal of Geological Society of London 118, 385–428.

Fossen, H., Tikoff, B., 1993. The deformation matrix for simultaneous simple shearing, pure shearing and volume change, and its application to transpression-transtension tectonics. Journal of Structural Geology 15, 413–422.

Ghosh, S.K., Ramberg, H., 1976. Reorientation of inclusions by combinations of pure shear and simple shear. Tectonophysics 34, 1–70.

Goscombe, B., Passchier, C.W., 2003. Asymmetric boudins as shear sense indicators-an assessment from field data. Journal of Structural Geology 25, 575–589.

Goscombe, B., Passchier, C.W., Hand, M., 2004. Boudinage classification: end-member boudin types and modified boudin structures. Journal of Structural Geology 26, 739–763.

Heilbronner, R., Tullis, J., 2006. Evolution of *c*-axis pole figures and grain size during dynamic recrystallization: Results from experimentally sheared quartzite. Journal of Geophysical Research 111, B10202, doi:10.1029/2005JB004194.

Hietanen, A., 1967. On the facies series in various types of metamorphism. Journal of Geology 75, 187–214.

Hippertt, J.F., 1993. V-Pull-apart microstructures: A new shear sense indicator. Journal of Structural Geology 15, 1393–1404.

Hudleston, P.J., 1999. Stain compatibility and shear zones: is there a problem? Journal of Structural Geology 21, 23–932.

Hynes, S.J., McQuillan, H., 1974. Evolution of the Zagros suture zone, southern Iran. Bulletin of Geological Society of America 85, 739–744.

Hynes, S.J., Reynolds, P.H., 1980. Early development of Tethys and Jurassic ophiolite displacement. Nature 283, 561–563.

Ofoegbu, G.I., Ferrill, D.A., 1998. Mechanical analyses of listric normal faulting with emphasis on seismicity assessment. Tectonophysics 284, 65–77.

Jeffery, G.B., 1922. The motion of ellipsoid particles immersed in a viscous fluid. Proceedings of the Royal Society London A 102, 161–179.

Jiang, D., Williams, P.F., 1998. High-strain zones: a unified model. Journal of Structural Geology 20, 1105–1120.

Jiang, D., Lin, S., Williams, P.F., 2001. Deformation path in high-strain zones, with reference to slip partitioning in transpressional plate-boundary regions. Journal of Structural Geology 23, 991–1005.

Jones, R., Holdsworth, R.E., Clegg, P., McCaffrey, K., Tavarnelli, E., 2004. Inclined transpression. Journal of Structural Geology 26, 1531–1548.

Law, R.D., 1990. Cystallographic fabrics: a selective review of their applications to research in structural Geology. In: Knipe, R.J., Rutter, E.H. (Eds.), Deformation Mechanisms, Rheology and Tectonics, Vol. 54. Geological Society Special Publication, pp. 335–352.

Law, R.D., Searle, M.P., Simpson, R.L.O., 2004. Strain, deformation emperatures and vorticity of flow at the top of the Greater Himalayan slab, Everest Massif, Tibet. Journal of the geological Society London 161, 305–320.

Lister, G.S., Dornsiepen, U.F., 1982. Fabric transitions in the Saxony Granulite Terrain. Journal of Structural Geology 4, 81–92.

Lister, G.S., Snoke, A.W., 1984. S–C mylonites. Journal of Structural Geology 6, 617–663.

Lisle, R.J., 1979. Strain analysis using deformed pebbles. The influence of initial pebble shape. Tectonophysics 60, 263–277.

Liu, X., McNally, K.C., Shen, Z.K., 1995. Evidence for a role of the down going slab in earthquake partitioning at oblique subduction zones. Journal of Geophysical Research 100, 15351–15372.

Marshak, S., Mitra, G., 1988. Basic Methods of Structural Geology. Prentice-Hall, Englewood Cliffs, NJ.

McClay, K.R. (Ed.), 1992. Thrust Tectonics. Chapman and Hall, London.

McClay, K.R., Insley, M.W., 1986. Duplex structures in the Lewis thrust sheet, Crows nest Pass. Rocky Mountains, Alberta, Canada. Journal of Structural Geology 8, 911–922.

McQuarrie, N., Stock, J.M., Verdel, C., Wernick, B.P., 2003. Cenozoic evolution of Neo-Tethys for the causes of plate motions. Geophysical Research Letters 30 (20), doi:10.1029/2003GL017992.

Means, W.D., 1994. Rotational quantities in homogeneous flow and development of small-scale structures. Journal of Structural Geology 16, 437–445.

Means, W.D., Hobbs, B.E., Lister, G.S., Williams, P.F., 1980. Vorticity and non-coaxiality in progressive deformations. Journal of Structural Geology 2, 371–378.

Mohajjel, M., Fergusson, C.L., 2000. Dextral transpression in Late Cretaceous continental collision, Sanandaj–Sirjan Zone, western Iran. Journal of Structural Geology 22, 1125–1139.

Okudaira, T., Takeshita, T., Hara, I., Ando, J., 1995. A new estimate of the conditions of the transition from basal <a> to prism [c] slip in natural deformed quartz. Tectonophysics 250, 31–46.

Passchier, C.W., 1987. Stable positions of rigid objects in non-coaxial flow: a study in vorticity analysis. Journal of Structural Geology 9, 679–690.

Passchier, C.W., 1988. Analysis of deformation paths in shear zones. Geolgisches Rundschau 77, 309–318.

Passchier, C.W., 1998. Monoclinic model shear zones. Journal of Structural Geology 19, 113–127.

Passchier, C.W., Trouw, R.A.J., 2005. Micro-Tectonics. Springer, Berlin.

Platt, J.P., Behrmann, J.H., 1986. Structures and fabrics in a crustal scale shear zone, Betic Cordilleras, SE Spain. Journal of Structural Geology 8, 15–34.

Platt, J.P., Leggeth, J.K., 1986. Strata extension in thrust footwalls Makran accretionary prism: implications for thrust tectonics. American Association of Petroleum Geologists Bulletin 70, 191–203.

Robin, P.F., Cruden, A., 1994. Strain and vorticity patterns in ideally ductile transpression zones. Journal of Structural Geology 16, 447–466.

Ramsay, J.G., 1967. Folding and Fracturing of Rocks. McGraw-Hill, New York.

Ramsay, J.G., Hubber, M.I., 1983. The Techniques of Modern Structural Geology. Volume 1: Strain Analysis. Academic Press, New York.

Ramsay, J.G., Hubber, M.I., 1987. The Techniques of Modern Structural Geology. Volume 2: Folds and Fractures. Academic Press, London.

Sanderson, D.J., Marchini, W.R.D., 1984. Transpression. Journal of Structural Geology 6, 449–458.

Samanta, S.K., Mandal, N., Chakraborty, C., 2002. Development of different types of pull-apart microstructures in mylonites: an experimental investigation. Journal of Structural Geology 24, 1345–1355.

Sarkarinejad, K., 1999. Tectonic finite strain analysis using: Ghouri deformed conglomerate, Neyriz area, Southwestern Iran. Iranian Journal of Science and Technology 23, 352–363.

Sarkarinejad, K., 2003. Structural and microstructural analysis of palaeo-transform fault zone in the Neyriz ophiolite, Iran. In: Dilek, Y., Robinson, R.T. (Eds.), Ophiolite in Earth History, Vol. 218. Geological Society, London Special Publication, pp. 129–145.

Sarkarinejad, K., 2005. Structures and microstructures related to steady-state mantle flow in the Neyriz ophiolite, Iran. Journal of Asian Earth Sciences 25, 859–881.

Sarkarinejad, K., 2007. Quantitative finite strain and kinematic flow analyses along the Zagros transpression zone, Iran. Tectonophysics 442, 49–65.

Schmid, S.M., Casey, M., 1986. Complete fabric analysis of some common observed quartz *c*-axis patterns. American Geophysical Union Monograph 36, 263–286.

Shahidi, A., Taraz, H., Zamani Pedram, M., Alavi, M., Parto Azar, H., 1999. Geological map of the Dehbid area, scale. 1:100000. Geological Survey of Iran, Tehran, Iran.

Sheikholeslami, R., Bellon, H., Emami, H., Sabzehei, M., Pique, A., 2003. Nouvelles données structurale et datations ^{40}K-^{40}Ar sur les roches métamorphiques de la region Neyriz (zone de Sanandaj–Sirjan, Iran meridional).Leur intéret dans le cadre du domaine néo-téthysien du Moyen-Orient. Geoscience 335, 981–991.

Simpson, C., De Paor, D.G., 1997. Practical analysis of general shear zones using the porphyroclast hyperbolic distribution method: an example from Scandinavian Caledonides. In: Sangupta, S. (Ed.), Evolution of Geological Structures In Micro- to Macro-Scales. Chapman and Hall, London, pp. 169–184.

Suppe, J., 1983. Geometry and Kinematics of fault bend folding. American Journal of Science 283, 684–721.

Suppe, J., 1985. Principles of Structural Geology. Prentice-Hall, Englewood Cliffs, NJ, 537 pp.

Stöcklin, J., 1968. Structural history and tectonics of Iran. American Association of Petroleum Geologists Bulletin 52, 1229–1258.

Stöcklin, J., 1974. Possible ancient continental margins in Iran. In: Burk, C.A., Drake, C.L. (Eds.), The Geology of Continental Margins. Springer, New York, pp. 873–888.

Takin, M., 1972. Iranian geology and continental drift in the Middle East. Nature 235, 147–150.

Tchalenko, J.S., Braud, J., 1974. Seimicity and structure of the Zagros (Iran): the Main Recent Fault between 33°and 35°N. Philosophical Transactions of the Royal Society London 227 (1262), 1–25.

Tikoff, B., Fossen, H., 1993. Simultaneous pure and simple shear: The unifying deformation matrix. Tectonophysics 217, 267–283.

Tikoff, B., Fossen, H., 1999. Three-dimensional reference deformations and strain facies. Journal of Structural Geology 21, 1497–1521.

Tikoff, B., Teyssier, C., 1994. Strain modeling of displacement-field partitioning in transpressional orogens. Journal of Structural Geology 16, 1575–1588.

Tripathi, A., Gairola, V.K., 1999. Fold symmetry: a quantitative description. Journal of Structural Geology 21, 719–727.

Twiss, R.J., Moores, E.M., 1992. Structural Geology. Freeman and Co., New York, 532 pp.

Vernant, P., Nilforoushan, F., Hatzfeld, D., Abbassi, M.R., Vigny, C., Masson, F., Nankali, H., Martinod, J., Ashtiani, A., Tavakoli, F., Chery, J., 2004. Present-day crustal deformation and plate kinematics in the Middle East constrained by GPS measurements in Iran and northern Oman. International Journal of Geophysics 157, 381–398.

Vernant, P., Chery, J., 2006. Mechanical modeling of oblique convergence in the Zagros, Iran. Geophysical Journal International 165, 991–1002.

Wallis, S.R., 1992. Vorticity analysis in a metachert from the Sanbagawa belt, SW Japan. Journal of Structural Geology 14, 271–280.

Wallis, S.R., Platt, J.P., Knott, S.D., 1993. Recognition of syn-convergence extension in accretionary wedges with example from the Calabrian arc and the Eastern Alps. American Journal of Science 293, 463–495.

Wells, A.J., 1969. The Crush Zone of the Iranian Zagros Mountains and its implications. Geology Magazine 106, 385–394.

White, S.H., 1979. Grain and sub-grain size variations across a mylonite zone. Contributions to Mineralogy and Petrology 70, 193–202.

Wilson, C.J.L., 1975. Preferred orientation in quartz ribbon mylonites. Geological Society of American Bulletin 86, 968–974.